Climate- and Weather-Driven Solid-Earth Deformation and Seismicity

Roland Bürgmann[1], Kristel Chanard[2], and Yuning Fu[2]

[1] Seismological Laboratory, University of California Berkeley, Berkeley, CA, United States
[2] Université de Paris-Cité, Institut de physique du globe de Paris, CNRS, IGN, F-75005 Paris, France
[3] School of Earth, Environment and Society, Bowling Green State University, Bowling Green, OH, United States

Book Chapter for "GNSS Monitoring of the Terrestrial Environment", Elsevier

Abstract

There is long-standing interest in the interactions between atmospheric and hydrological processes and solid Earth deformation, including the occurrence of earthquakes. Here, we review evidence for the effects of climatic processes and weather on deformation and seismicity in the lithosphere over a wide range of time scales, ranging from load cycles associated with the ice ages to the effects of short-term weather events. Space- and ground-based geophysical observations allow us to capture the redistribution of surface loads in the form of water, ice, and sediments, as well as near-surface pressure and temperature changes in the atmosphere and varying fluid pressure in the shallow subsurface. While earthquakes are generally the result of tectonic or volcanic activity, the climatic forcings induce stress changes on faults that in some cases can be shown to significantly encourage or retard the occurrence of earthquakes, depending on the degree to which the external forces align with the background tectonic stress field. Stress changes associated with the emplacement and removal of km-thick ice sheets and lakes are large enough to substantially change slip- and earthquake rates on major plate-boundary faults and can also trigger events in largely aseismic continental interiors. However, climate-earthquake interactions are subtle and proving the interaction between climate and earthquakes requires careful mechanical modeling and statistical analysis. While investigations of earthquake weather and climate are not likely to be relevant for the characterization and mitigation of earthquake hazard, they provide important insights into the physical processes associated with lithospheric deformation, the earthquake cycle and frictional faulting in the Earth.

Key Words: Climate and Weather; Hydrology; Seismicity; Deformation; Stress; Earthquake Triggering and Modulation; Surface Loading; Geodesy

1 Introduction

Earth's surface represents the interface of the lithosphere, the outer layer of the solid Earth, with the cryosphere, hydrosphere and atmosphere. Surface processes, including the hydrological cycle and the erosion, transport and deposition of sediments, reflect the effect of climate and weather on the solid Earth. Tectonics and crustal deformation, in turn, can affect climate and weather by reshaping Earth's topography. Thus, the lithosphere and the atmosphere may interact over a range of time scales, from billions of years (associated with the compositional evolution of the atmosphere, the formation and growth of continents, and plate tectonics), to seconds (associated with storm events, earthquakes, and volcanic eruptions). Mankind has long been fascinated by the possibility of atmospheric and hydrological processes (i.e., climate,weather and the hydrological cycle) affecting solid Earth deformation processes in the brittle lithosphere, including earthquakes that are generally understood to mostly be a result of plate tectonics. For good reasons, the idea of "earthquake weather"; that is, a particular weather pattern or season in which earthquakes preferably occur, has generally been considered an urban myth (e.g., Fallou et al., 2022).

Recent advances in geophysical observations, including the Global Navigation Satellite System, GNSS, have revealed significant deformation associated with climate and weather (e.g., White et al., 2022), which is superimposed on plate tectonic and earthquake cycle deformation. Processes involved in this atmospheric forcing of solid Earth deformation include the redistribution of surface loads via sediments, water and ice, near-surface pressure and temperature changes in the atmosphere, and varying fluid pressures in the shallow subsurface (Figure 1). Deformation associated with changes in surface loads and poroelastic and thermoelastic eigenstrains associated with changes in subsurface fluid pressure and temperature will also perturb the state of stress on faults at depth. Depending on how close such faults are to their critical failure stress and to what degree the climate-driven stress changes encourage or discourage failure, we may thus expect some effect on the distribution of earthquakes in space and time.

Tectonic stressing rates in plate boundary zones are on the order of 1-100 kPa/yr, and substantially less in intra-continental regions. Earthquakes typically cause a drop in stress of about 1 to 100 MPa, but the absolute ambient stress is rather poorly known, with an upper bound provided by the frictional strength of faults (Byerlee, 1978). Atmospheric processes drive hydrological and sedimentary mass transport and produce changes in temperature and fluid pressure in the shallow Earth, which modify subsurface stress over a wide range of spatial and temporal scales (Figure 2). The addition or removal of a meter-thick layer of water or ice on the Earth's surface adds or subtracts a vertical load of about 10 kPa and the most extreme atmospheric pressure drops associated with tropical cyclones can also approach 10 kPa. Thus, while stresses caused by atmospheric and hydrological processes are generally small compared to those from the unrelenting forces associated with plate tectonics, they can cause substantial variations in stressing rates and may thus change the distribution of seismicity in space and time. Of course, lake- or sea-level changes of many tens of meters or the growth and retreat of glaciers and ice sheets many hundreds of meters thick will have an even greater effect on solid Earth deformation and stress. Here, we review recent advances in our understanding of climate- and weather-driven solid-Earth deformation, stress and seismicity. We consider time scales ranging from a hundred thousand years (associated with ice age cycles) to days (associated with daily weather events). We find that while most earthquakes are the result of tectonic processes, the occurrence of a small but significant number of earthquakes appears to have been accelerated, delayed or modulated by atmospheric and hydrological processes.

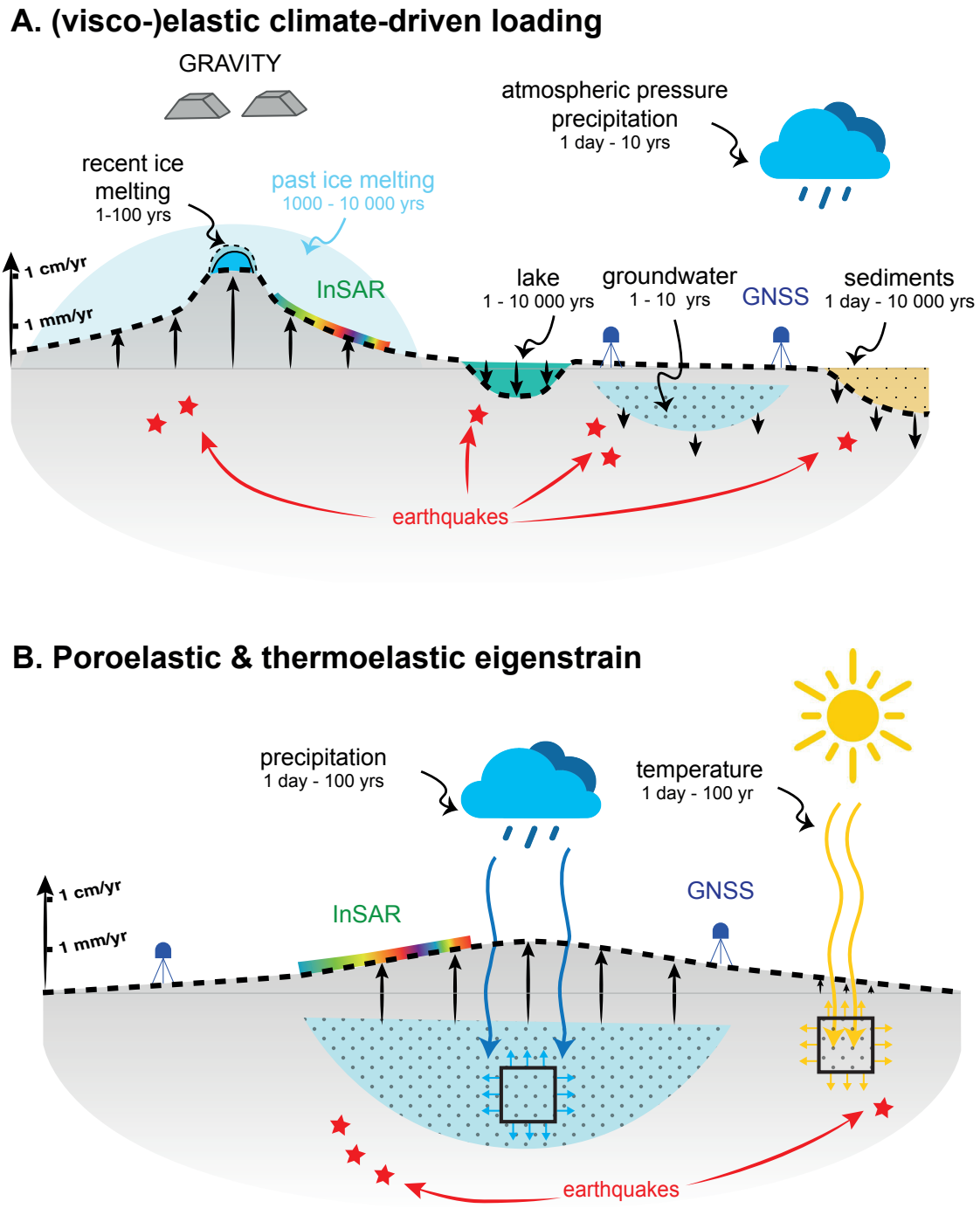

Figure 1: Deformation and stresses due to climate-driven surface loading and poro- and thermoelastic eigenstrain. (A) Schematic representation of the effect of various processes involving past and present surface and subsurface loading, including Glacial Isostatic Adjustment (GIA) in response to unloading of the last glacial maximum ice cap, recent ice melting, lake loading, groundwater, precipitation, atmospheric pressure, and sediments. (B) Schematic representation of the effect of poroelastic and thermoelastic eigenstrain induced by fluctuations in groundwater level and surface temperature. Geodetic measurements by GNSS, InSAR and space-based gravity illuminate these processes.

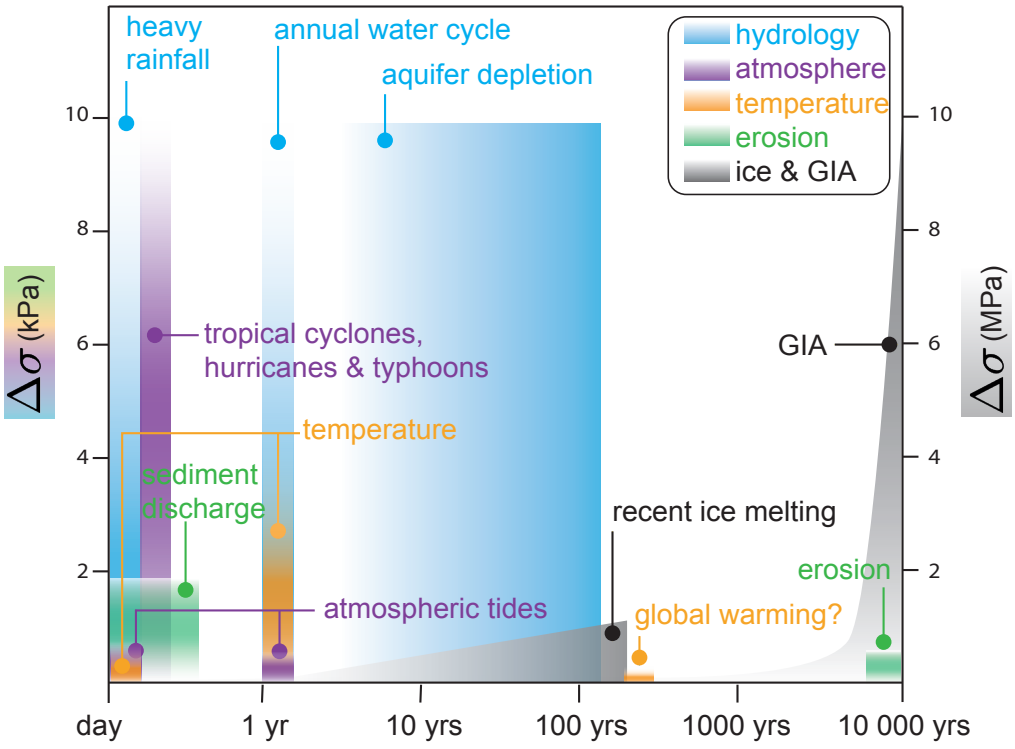

Figure 2: Timescales of climate-driven surface processes and associated stress variations. Note the substantially higher peak stress changes of several MPa associated with ice sheet loading and glacial isostatic adjustment (GIA, right y-axis), compared to atmospheric, hydrological, erosional, and thermally induced stress changes of a few kPa that occur on shorter time scales (left y-axis).

2 Observing and Modeling Climate-driven Deformation, Stress and Seismicity

2.1 Measuring climate-driven deformation

The solid Earth deforms in response to climate-driven spatial and temporal changes in surface mass load, including terrestrial water storage, ice, snow, and sediment transport through landsliding and erosion (Figure 1A). Additionally, temperature variations near the Earth's surface and pressure fluctuations in groundwater are associated with thermoelastic and poroelastic eigenstrain in the shallow Earth, which also causes the solid Earth to deform (Figure 1B). Using space geodetic observations, it becomes possible to comprehensively capture and constrain models of these mass load changes and deformation processes (Figure 1).

Measuring climate-driven mass load changes has been enabled by the launch of the Gravity Recovery and Climate Experiment (GRACE; 2002-2017) and GRACE Follow-On (GRACE-FO, 2018-in orbit) satellite missions which introduced a unique observable: monthly global measurements of Earth's space and time-varying gravity field at a spatial resolution of 300-400 km (Tapley et al., 2004; Landerer et al., 2020). By combining GRACE-derived mass loads with a (visco-)elastic Earth model through the load Love numbers theory, it is possible to compute the loading-induced deformation of the Earth (Farrell, 1972; Cathles, 1975), which can be compared to independent GNSS measurements.

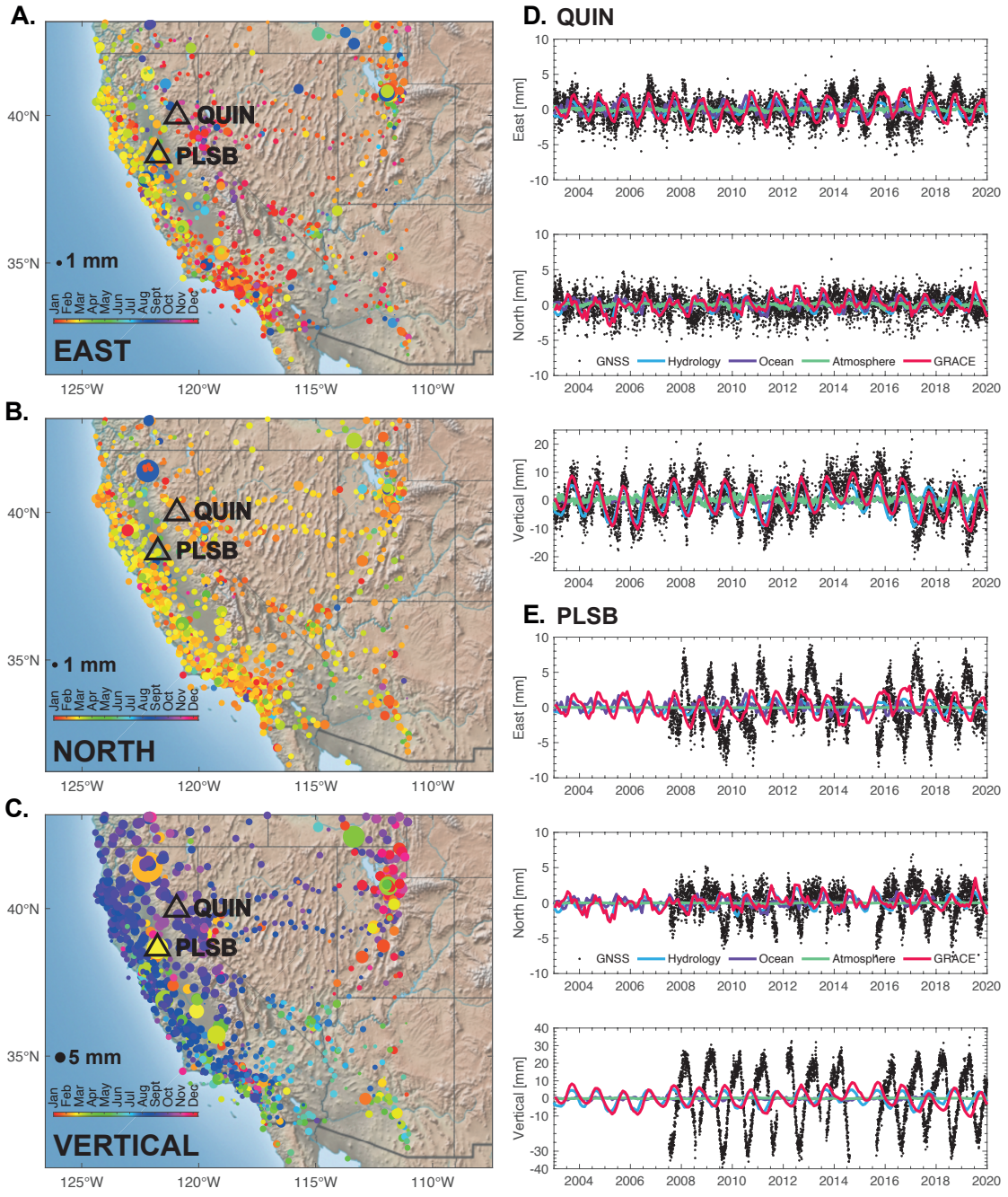

Figure 3: Amplitude and phase of maximum (A) East, (B) North and (C) Vertical annual displacements in the Southwestern US, estimated from GNSS time series processed by the Nevada Geodetic Laboratory (Blewitt et al., 2018) aligned to the IGS14 reference frame (Altamimi et al., 2016). Black triangles highlight GNSS stations QUIN and PLSB, located in the Sierra Nevada mountain range and above the Sacramento aquifer system, respectively. Detrended daily East, North and Vertical positions time series at these two GNSS stations are shown in (D) and (E) with deformation models derived from, in blue, hydrological (GLDAS; Rodell et al., 2004), in green, atmospheric (ERA5; Hersbach et al., 2020), in purple, non-tidal oceanic (ECCO; Wunsch et al., 2009) and in red, GRACE/-FO load (Gauer et al., 2023).

Climate-induced deformation of the Earth's surface can be directly measured using geodetic observations (Figure 3). GNSS stations measure positions and changes in position at millimeter-level accuracy. Time series of GNSS stations have been used to investigate the, primarily elastic, solid Earth's response to global (e.g., Blewitt et al., 2001; van Dam et al., 2001; Dong et al., 2002) and regional seasonal and long-term variations in continental water storage, and within the atmosphere and ocean. Regional examples include seasonal hydrological loading deformation in the Amazon River basin (e.g., Davis et al., 2004; Bevis et al., 2005; Knowles et al., 2020) and the Nepal Himalaya (e.g., Fu and Freymueller, 2012a; Chanard et al., 2014), snow cover in Japan (Heki, 2004) and Iceland (Grapenthin et al., 2006; Compton et al., 2015).. In the western US, snow and rainfall cause strong seasonal deformation, reaching up to a few mm and a few cm horizontal and vertical annual amplitude, and drought periods induce multi-year signals of similar amplitudes (Figure 3; e.g. Ouellette et al., 2013; Argus et al., 2014; Borsa et al., 2014; Amos et al., 2014; Fu et al., 2015). In addition to hydrological loads, the change in atmospheric pressure loading causes deformation of the Earth (Darwin, 1882; van Dam and Wahr, 1987). van Dam et al. (1994) analyzed daily GNSS time series and concluded that atmospheric loading displacements accounts for up to 24% of the total variance in GNSS height series.

At the global scale (Chanard et al., 2018a) and in regions of large-scale hydrological, atmospheric and non-tidal oceanic mass variations (Davis et al. 2004; van Dam et al., 2007) captured by GRACE/-FO, predicted surface displacements using a purely elastic spherical and layered Earth model (Dziewonski & Anderson, 1981)s are in good agreement with GNSS observations (Figure 3D). However, discrepancies at the regional scale exist, unlikely to be related to the choice of Earth's mechanical properties (Chanard et al., 2018b). These discrepancies may be due to the high noise level of GRACE/-FO products (e.g. Chen et al., 2022) or its coarse spatial resolution (350 km) compared to GNSS observations. Moreover, as GRACE measures integrated mass variations, and distinguishing between sources of mass change at the Earth's surface versus within its interior is critical to correctly infer climate-driven deformation from gravity measurements (e.g. Chen et al., 2022). Environnemental models, including hydrological, atmospheric and non-tidal oceanic loads, provide sources of deformation independently and present higher spatio-temporal resolution but, similar to GRACE-derived models, their combination can explain only up to 50% of the observed seasonal vertical displacements and up to 20% of the horizontal ones (Figure 3D; e.g. Li et al., 2016).

Greater details of surface loading can be mapped by inverting ground deformation recorded by dense GNSS networks. For example, using the EarthScope Plate Boundary Observatory (PBO) GNSS data, climate-related terrestrial water storage variations have been quantified at high spatial resolution (tens of kilometers) in California (Amos et al., 2014; Argus et al., 2014; 2017; Johnson et al., 2017a), the Pacific Northwest (Fu et al., 2015), and across the western United States (Borsa et al., 2014; Enzminger et al., 2018). These studies captured both annual cycles of water load as well as multi-year variations associated with regional drought conditions. Milliner et al. (2018) extended this technique to load variations over the course of a few days and estimated the total water mass released by Hurricane Harvey at the Texas Gulf Coast. Yet, the method is limited to well-instrumented regions, with a resolution that depends on the (often uneven) inter-station distances and may not capture the full load complexity (Wahr et al., 2013). Moreover, results may be biased by other geophysical signals or systematic errors polluting GNSS observations (Chanard et al., 2020; Larochelle et al., 2022).

Other geophysical signals recorded by GNSS stations include poroelastic deformation driven by fluctuations in groundwater level and thermoelastic strain due to spatiotemporal variations of near-surface temperature (Figure 4). When surface hydrological loading increases, it can also lead to downwards fluid infiltration and diffusion, causing pore pressure and thus, the Coulomb stress to rise. It can also enhance hydrofracturing in favorably oriented cracks. While surface hydrological loading has been established as the primary source of GNSS seasonal observations, the contribution of poroelastic processes to surface deformation has received renewed attention in

recent years. The decametric resolution and mm/yr accuracy of Interferometric Synthetic Aperture Radar (InSAR) make it a powerful tool to monitor localized surface subsidence in response to groundwater depletion (e.g., Amelung et al., 1999; Chaussard et al., 2014, Ojha et al., 2018). GNSS provides valuable complementary observations to monitor poroelastic deformation, offering a better temporal resolution, a more accurate separation of horizontal and vertical displacements, and the potential to identify errors specific to each geodetic technique (Larochelle et al., 2022). However, while surface loading models generally agree with observations of non-linear motion at GNSS sites anchored to bedrock (Figure 3D), they fail at predicting the amplitude and phase of site motion when located on or around groundwater basins (Figure 3E). Additionally, fluctuations in surface temperature that can span tens of degrees annually cause the shallow Earth to deform thermoelastically, with differential motions of up to several millimeters (Prawirodirdjo et al. 2006; Ben-Zion & Allam 2013; Xu et al., 2017). Poroelastic and thermoelastic processes are now well recognized, but their modeling remains challenging and further research is needed to fully comprehend and model the link between changes in groundwater, temperature and surface deformation.

2.2 Modeling climate-driven deformation and stress

Mechanical models are needed to quantitatively relate surface loads to Earth deformation and stress (Figure 4). In the 3D, semi-infinite, homogeneous elastic solid approximation, analytical solutions exist for strain and stresses caused by a surface point load (Boussinesq, 1885). These solutions have been used to model stresses on faults induced by seasonal hydrology (Bettinelli et al., 2008) or erosion (Steer et al., 2014). The solution of deformation by surface loads on a more realistic spherical elastic Earth model was provided by Farrell (1972) following the method of Longman (1962 and 1963). Load Love numbers and the resulting Green's functions can be computed based on a spherical, radially stratified Earth model (e.g., Wang et al., 2012), such as the PREM (Preliminary Reference Earth model, Dziewonski and Anderson, 1981). The loading-induced stress changes in the Earth can then be calculated combining strain and the elastic moduli of the Earth. Many programs have been developed to compute elastic strain induced by surface loading in the spherical Earth approximation. For example, SPOTL is designed to calculate ocean tidal loading (Agnew, 1997) but can be utilized to calculate deformation induced by surface loads (e.g., Borsa et al., 2014). STATIC1D (Pollitz, 1996) can be used to model strain and stress from a surface load force (e.g., Johnson et al., 2017a and 2017b). LoadDef models elastic deformation by surface mass loading for any planetary body (Martens et al., 2019). ISSM-SESAW is especially designed for cryospheric loading problems of ice and glaciers (Adhikari et al., 2016) and REAR is another simulation tool to model loading deformation by cryospheric loads (Melini et al., 2014). These spherical models can be extended to the viscoelastic domain for Newtonian rheologies, including Maxwell and Burgers bodies, which are necessary to investigate deglaciation-induced strain and stress fields through time (Wu et al., 1999; Wu and Johnston, 2000; Lambeck and Purcell, 2003; Pollitz et al., 2013; Craig et al., 2016; Michel & Boy, 2022). In addition to analytical solutions, programs relying on the finite element method, such as Pylith (Aagaard et al., 2017), have been developed to compute more detailed loading-induced strain and stress of the Earth by surface forces, but are often limited to a smaller region (Hampel et al., 2009; Lund et al., 2009; Brandes et al., 2015).

Models also exist that allow for computing deformation and stress from subsurface fluid pressure changes caused by the infiltration of surface water. These include simple point pressure sources (Mogi, 1958), solutions of finite strain cuboid sources in a homogeneous half-space (Barbot et al., 2017), analytical solutions for an unconfined aquifer with heterogeneous elastic properties (Larochelle et al., 2022), and numerical solutions of the poroelastic problem (Wang and Kümpel, 2003). In the upper few kilometers of the crust, strain and stress changes from the poroelastic response to groundwater level changes greatly exceed those from hydrological surface loading, but rapidly decay with increasing depth (e.g., Miller, 2008; Hu and Bürgmann, 2020).

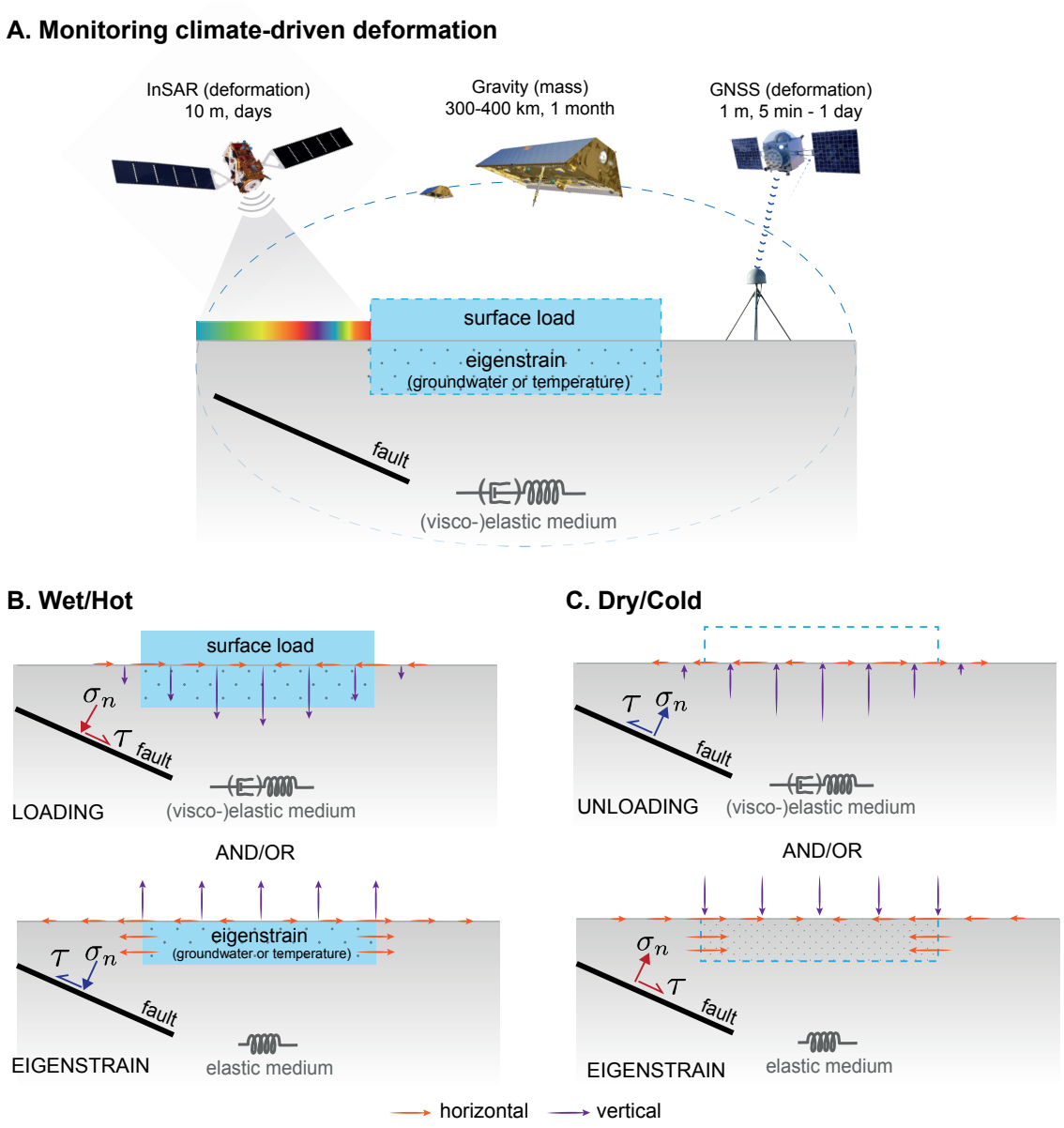

Figure 4: (A) Schematic illustration of space-geodetic observations and models of hydrologically induced deformation and stress changes. (B) During a wet season, an increase of near-surface water load (surface and groundwater, ice and snow) causes 3D loading displacements and also applies normal (σ_n) and shear (τ) stress changes on a nearby fault, thus inducing Coulomb stress changes ($CS = \tau + \mu\sigma_n$, where μ is the fault friction coefficient; Stein et al., 1999). An increase of subsurface groundwater also results in an expansion and elevated pore fluid pressure, which may also lead to Coulomb stress change on an adjacent fault. Similarly, zones of high temperature produce thermoelastic eigenstrains and stresses. (C) The opposite scenario occurs during a dry/cold period.

Poroelasticity and thermoelasticity are based on the same mathematical framework (Biot, 1956; Rice and Cleary, 1976; Tsai, 2011). The problem of thermoelastic eigenstrain and stresses has been relatively well studied, particularly due to its importance in material sciences. Berger (1975) provided a solution to describe thermoelastic strain in a 2-D homogeneous elastic half-space, induced by spatially and temporally periodic surface temperature variations. Ben-Zion and

Leary (1986) extended this solution to the case of an elastic half-space covered by a thin layer of unconsolidated incompetent material, and the model was further developed and applied by Tsai (2011). The thermoelastic problem has only recently been tackled for geophysical applications in a spherical frame, which is more suited for large-wavelength or global studies (Fang et al., 2014).

The Coulomb failure criterion has been widely applied to quantify the stress condition required for a fault to rupture. Coulomb stress change can be simplified as $\Delta CS = \Delta\tau + \mu\Delta\sigma_e$, where $\Delta\tau$ is the shear stress change, $\sigma_e = \sigma_n - p$ is the effective normal-stress change (i.e., the difference between the normal stress σ_n and pore pressure p), and μ is the fault friction coefficient (Stein et al., 1999). Positive Coulomb stress change is considered to promote fault failure and negative Coulomb stress change suppresses failure. Under undrained conditions, the change in pore pressure due to a change in normal stress is given by $\Delta p = B\Delta\sigma_n$, where B is the Skempton coefficient (and typically ranges between 0.5 and 0.9). Thus, $\Delta CS = \Delta\tau + \mu\Delta\sigma_n(1 - B)$. Because of fluid flow, the induced pore pressure changes are time-dependent and it becomes important to consider the timescale for which a poroelastic stress change model is applied (e.g., Cocco and Rice, 2002).

2.3 Documenting earthquake triggering and modulation

The idea that climate might influence seismicity dates back to at least the fourth century B.C., when Aristotle proposed that winds trapped in subterranean caves generated earthquakes (Missiakoulis, 2008). Since the early twentieth century, studies have suggested that climate-driven transient and oscillatory stresses may be sufficient to trigger or modulate seismicity given the slow buildup of stress along active faults (Figure 5A; Drake, 1912; Sayles, 1913; Taber, 1914). However, establishing correlations between climate forcing and seismicity is challenging because it requires quantitative or statistical methods, high-quality data sets, and extended observation periods. A number of studies have investigated temporal changes in the statistics of recorded seismicity, such as earthquake frequency, seismic moment rate or the b-value of the Gutenberg-Richter earthquake frequency-magnitude distribution, in relation to climatic events or periodic forcing (e.g., Zhai et al., 2021).

Several statistical approaches, continuous or discrete in time, have been shown to be effective at detecting periodicities in seismic catalogs. The Schuster test (Schuster, 1897), and its recent extension, the Schuster spectrum (Figure 5B; Ader and Avouac, 2013), use the relative discrete timing of seismic events for statistical analysis. The probability that the temporal distribution of events is periodic at a given frequency is compared to the null hypothesis, where the event distribution arises from a uniform seismicity rate. Other approaches exist, based on the use of time series analysis and periodogram statistics, such as the unifrequential Schuster periodogram (Schuster, 1898) or its multi-frequential extension and generalization, the multi-frequential periodogram (Dutilleul, 2015), which can detect overlapping signals with fractional frequencies. However, periodograms require a trigonometric model hypothesis. Hsu et al. (2021) use the empirical mode decomposition to separate seismicity rate time series into signals with different time scales (intrinsic mode functions), focusing on annual and interannual variations. If the period of the external forcing is known (e.g., annual climate cycles), simple stacks or histograms of event occurrences are also commonly used (Figure 5A; e.g., Taber, 1914; Bollinger et al. 2008; Craig et al. 2017).

All these methods are subject to the implicit mathematical assumption of independent earthquake occurrences, and therefore can be biased by the occurrence of clustered aftershocks. As a result, statistical analysis of periodicities generally requires first declustering the seismic catalog through procedures relying on judgment-based parameter choices (e.g., Reasenberg, 1985; Zhuang et al., 2002; Zaliapin and Ben-Zion, 2020), which may impact the inference of periodicities (Dutilleul et al., 2015; Ueda and Kato, 2019).

In addition to applying statistical techniques to the temporal distribution of earthquakes, Johnson et al. (2017a; 2020) quantified the percentage of earthquakes that exceed the background

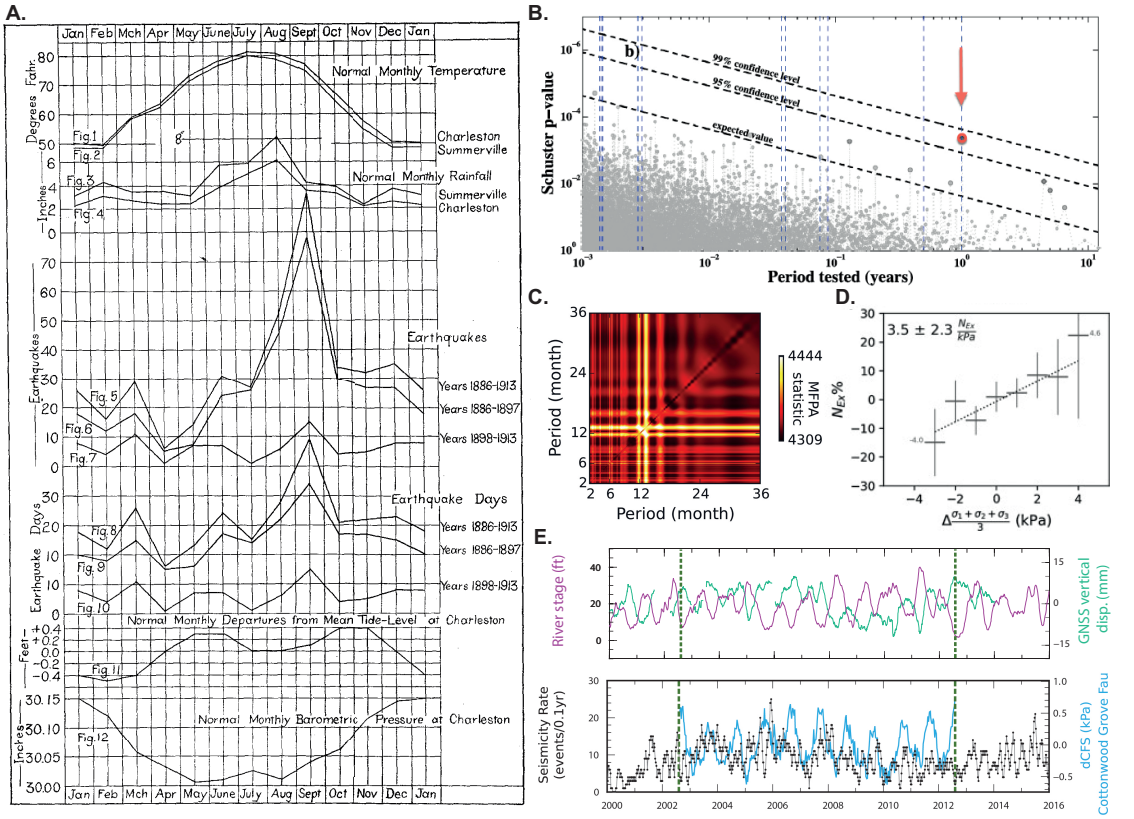

Figure 5: Examples of methods to detect seismic modulation by climate forcing. (A) Seasonal variations in temperature, precipitation, number of earthquakes and days with earthquakes (to reduce aftershock bias), oceanic and atmospheric pressure in South Carolina over the 1886-1913 period (Figure from Taber, 1914). (B) Seasonal periodicity of the Mb$\geq$ 4 mid-crustal Nepal seismic events from a Schuster spectrum of the 1965-2008 ISC seismic catalog (Figure from Ader and Avouac, 2013). (C) Seasonal periodicity of seismicity from the 1988-2002 Central San Andreas Fault near Parkfield seismic catalog inferred from contour maps of the multifrequential periodogram analysis in the bifrequential case. Here, the lighter the color, the higher the statistical significance of the detected periodicity (Dutilleul et al., 2015). (D) Percent excess seismicity of the 2000-2016 southern Alaska seismic catalog assuming a 3-month lagged response to hydrologically-driven differential stress variations, suggesting a delayed modulation mechanism (Johnson et al., 2020). (E) Correlation between the New Madrid region seismicity rate (black), variations in the Mississippi river stage, local GNSS vertical displacement and calculated Coulomb failure stress variations from GRACE loading variations on the Cottonwood grove fault (Craig et al., 2017).

seismicity rate with regard to climate-driven stress perturbations that encourage slip on known faults or enhance the background stress field to assess seismic modulation. Similarly, Craig et al. (2017) investigated correlations between seismicity rates and hydrology-driven stress variations on faults computed from satellite gravity measurements. These methods take faulting style and orientation into consideration when determining whether or not climatic forcing increases or decreases stress and seismic activity on faults.

3 Deformation and Seismicity from Changing Climate and Weather

3.1 Ice age climate cycles

Starting about 2.6 million years ago, Earth's climate has been dominated by ice age cycles accompanied by the emplacement and retreat of vast ice sheets and associated global sea level changes of over 100 m. In addition to ice sheets reaching far across high-latitude and elevated continental regions, large lakes at lower latitudes have also undergone correlated filling cycles. This cyclic global water redistribution, as well as associated erosion, transport and deposition of sediments, led to substantial changes in loading at the Earth's surface and stress under and surrounding continental ice sheets and lakes (e.g., Gilbert, 1890; Johnston, 1987), as well as in near-coastal regions (e.g., Luttrell and Smith, 2010). Since the end of the last ice age 12,000 years ago, the Earth has been adjusting to the associated removal of vast ice sheets and sea level rise through glacial isostatic adjustment (GIA), which, due to the time-dependent viscoelastic relaxation of the Earth's mantle, is an ongoing process evident in GNSS-measured deformation, GRACE measured gravity changes, and coastal sea level variations captured by raised shorelines and tide gauges (e.g., Milne et al. 2001; Caron et al., 2018; Sella et al. 2007; Tamisiea et al., 2007; Kierulf et al. 2021; van Dam, 2022, this volume) . Depending on the tectonic setting and associated lateral variation of the lithospheric thickness and effective mantle viscosity, the amplitude, duration, rate, and sign of GIA-induced deformation and associated stress changes are highly variable (e.g., Steffen et al., 2014; Wu et al., 2021; Vachon et al., 2022 and references therein).

Stress changes induced by GIA can reach more than ten MPa near, and in the forebulge of, the continental ice-sheet load zones (Figure 6), reaching deep into the lithosphere (e.g., Wu and Johnston, 2000; Wu et al., 2021; Vachon et al., 2022). As these stress changes can reach the range of typical earthquake stress drops, they are capable of triggering earthquakes on faults suitably oriented with respect to the induced stress field, or arrest slip on unfavorably oriented faults (e.g., Steffen and Steffen, 2021). Large prehistoric earthquake ruptures and current seismicity in Scandinavia, Greenland, North America, the European Alps, and around Antarctica have been linked to these large and enduring climate-driven stress changes (e.g., Wu and Johnston, 2000; Ivins, 2003; Steffen et al., 2020; Steffen et al., 2021; Wu et al., 2021; Vachon et al., 2022, and references therein). In the near field, triggered earthquake activity likely was most intense during and shortly after the latest pulse of deglaciation (e.g., Figure 6B), but enhanced seismicity in the previously glaciated areas appears to continue into the present, both in North America and Fennoscandia (Figure 6E). Glacial-load stresses may also suppress earthquake activity if they counteract the applied tectonic stress field, moving faults further away from critical failure stress conditions (e.g., Johnston, 1987). Activity in the forebulge during loading and ice-sheet advance is also observed (e.g., Pisarska-Jamroży et al., 2018; Steffen & Steffen, 2021; Štepancíková et al., 2022). Štepancíková et al. (2022) document a case of fault-slip acceleration during the peak glaciation phase in the Late Pleistocene on a fault in Central Europe 150 km from the ice sheet margin. This active period was followed by a cessation of activity throughout the Holocene, consistent with stress-change conditions in the forebulge, favoring slip during loading, rather than unloading.

Glacially triggered earthquakes generally reflect the combined effect of plate tectonic stresses and glacially induced isostatic stresses. It is often difficult to ascertain a direct relationship between GIA and earthquake occurrence, and thus some caution is warranted in assessing proposed triggering relationships, especially for events at large distances from the former ice sheet margin (e.g., Wu and Johnston, 2000; Steffen et al., 2021), such as the New Madrid seismic zone in North America. Even in Fennoscandia, the correlation of modeled current stress conditions with active seismicity is not simple, suggesting that other factors, such as unfavorable fault orientations and stress heterogeneity remaining from pre-glaciation conditions and earlier large triggered events (e.g., Gregersen et al., 2021), may influence the stress field (e.g., Wu et al., 1999). Nonetheless,

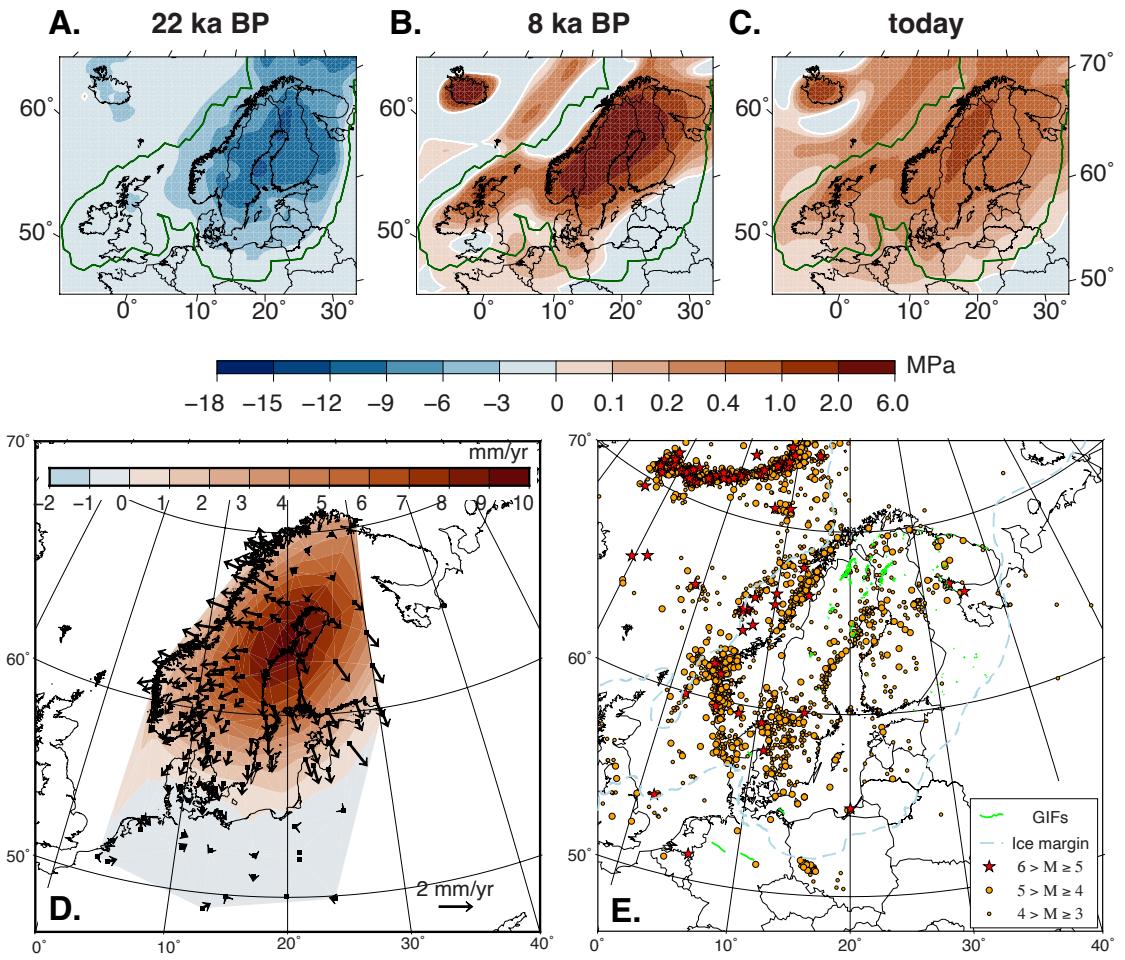

Figure 6: Stress, surface deformation and earthquakes associated with glacial isostatic adjustment in Fennoscandia. Change in Coulomb stress at 2.5 km depth from viscoelastic model calculation at (A) Last Glacial Maximum (22 ka), (B) soon after the ice sheet has completely melted (8 ka), and (C) present day (modified from Wu et al., 2021 and Patrick Wu, pers. comm., 2022). The green solid line shows the maximum ice sheet extent at Last Glacial Maximum. The numerical model assumes a background thrust-faulting stress regime with a N150°E-oriented maximum horizontal stress (see Wu et al., 2021 for details). Assuming zero Coulomb stress before glaciation, thrust faults were stabilized during maximum ice sheet loading, strongly encouraged to slip immediately following unloading, and continue to be loaded due to ongoing viscoelastic rebound. (D) Current vertical and horizontal surface velocities measured with GNSS (modified from Kierulf et al., 2021 and Holger Steffen, pers. comm.). (E) Glacially induced faults (GIFs) (green lines, from Munier et al., 2020) and recent ($M > 3$) seismicity. The dashed blue lines show the ice margin at Last Glacial Maximum (modified from Kierulf et al., 2021 and Holger Steffen, pers. comm.).

the clear evidence of glacially triggered earthquakes since the Last Glacial Maximum (e.g., Steffen et al., 2021) suggests that the ongoing shrinkage of many modern ice sheets owing to recent global warming could impact earthquake occurrences in these regions (e.g., Hampel et al., 2010; Sauber et al., 2021; Pagli et al., 2008).

The filling and desiccation of large lakes associated with glacial climate cycles also represent substantial surface loads and lead to deformation and redistribution of stress in the subsurface.

Lithospheric rebound due to the regression of Lake Bonneville in Utah, together with deglaciation and unloading of the nearby Rocky Mountains, may have nearly doubled fault slip rates and earthquake occurrences on normal faults in the eastern Basin and Range Province, in the early Holocene (Friedrich et al., 2003; Hetzel and Hampel, 2005; Hampel et al., 2010). Lake filling cycles in the Salton Trough basin in southern California during the last few thousand years have also been correlated with seismicity in an underlying fault-stepover zone and earthquake cycles on the nearby San Andreas fault, pointing to a direct linkage of earthquake hazard and climate-induced stresses (Brothers et al., 2011; Hill et al., 2023). Hill et al. (2023) proposed that the past six major events on the southern San Andreas Fault took place when the water level of Lake Cahuilla was high, which increased Coulomb stress on the fault by several hundred kPa and stressing rate by a factor of two.

In addition to the rapid retreat of the continental ice sheets and shrinking of large lakes in the early Holocene, associated rapid sediment transport may also produce substantial changes in surface loads that may trigger seismicity. For example, Calais et al. (2010) propose that $M > 7$ earthquakes in the intra-continental New Madrid seismic zone, which repeatedly occurred since the last ice age, resulted from unloading stresses associated with the accelerated fluvial erosion in the Mississippi River valley in the late Pleistocene, rather than from the direct or indirect far-field effects of the glacial unloading (Grollimund and Zoback, 2001; Pollitz et al., 2001). Similarly, Stein et al. (1989) and Gradmann et al. (2018) conclude that rapid coastal erosion and sediment transport during Pleistocene glaciations was a dominant source of stress changes in northern Norway.

As the massive ice sheets melted away at the end of the Pleistocene, sea level rose globally by 120 m at rates of 10–20 mm/yr, thus adding a substantial surface load in the ocean basins and along coastal margins (e.g., Lambeck and Chappell, 2001). The consequent elastic flexure produced shear stress changes in near-coastal regions reaching 1 MPa (Luttrell and Sandwell, 2010; Brothers et al., 2013). Lutrell and Sandwell (2010) use viscoelastic stress-modeling to find that nearshore (within a few hundred km) transform faults, such as the San Andreas, North Anatolian and Alpine fault systems experienced failure-encouraging stress increments (Figure 7), thus temporarily increasing their slip rate and decreasing earthquake recurrence intervals. However, they find that given the long timespans over which these stress changes occur, the stressing rates due to this process are modest compared to the rapid tectonic loading rates on the major strands of the plate-boundary faults. On the other hand, earthquake cycles on secondary, slow-slipping faults may have been more substantially perturbed. On the North Anatolian fault zone, where loading-induced stressing rates were order-of-magnitude higher due to the very sudden filling of the Black Sea, it is plausible that the high stressing rates led to seismic failure of much of the fault zone within a relatively short time. This possibly led to the observed synchronized timing of large earthquakes on the North Anatolian fault zone (Luttrell and Sandwell, 2010). On the Cascadia subduction zone, the shallow and coupled offshore megathrust was exposed to increased compression and thus slip is discouraged during sea level rise, whereas slip on the creeping downdip portion of the fault beneath the continent is accelerated (Lutrell and Sandwell, 2010). The associated stress changes on the subduction thrust are relatively small, but they could possibly affect the depth extent of ruptures during times of high versus low sea level (Luttrell and Sandwell, 2010). Brothers et al. (2013) propose that abundant slope failures observed in the sedimentary records of passive continental margins around 15 ka – 8 ka were caused by the seismic reactivation of suitably oriented and near-critically stressed near-coastal normal faults. Depending on the local tectonic environment, fault geometries and rate of stress associated with ice-age sea level change, earthquake cycles on nearshore faults may be substantially perturbed, especially on slow-moving faults for which the climatically induced stress changes are proportionally higher.

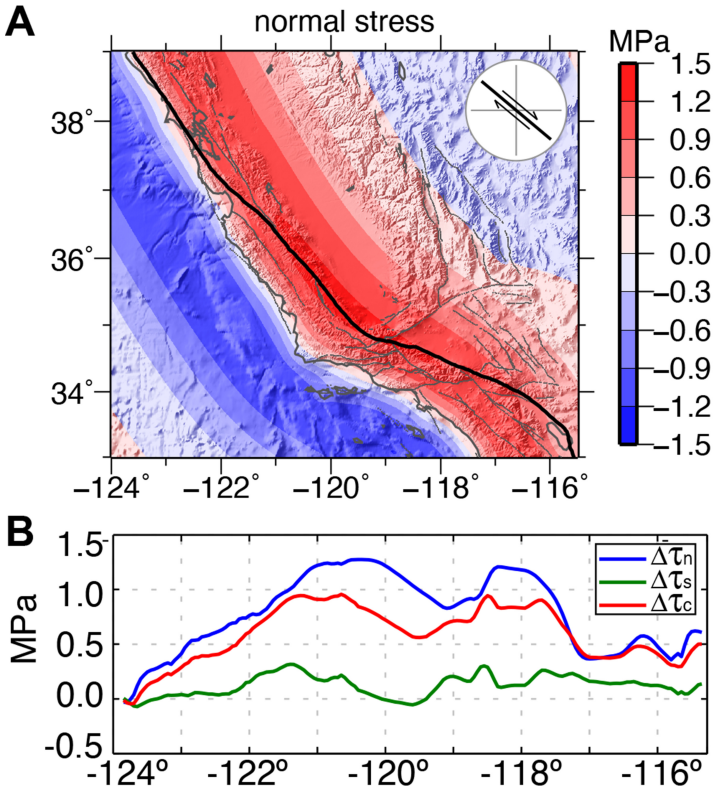

Figure 7: Stress perturbation on San Andreas fault system due to sea level rise since Last Glacial Maximum. (A) Normal-stress change (positive values represent slip-encouraging tension) on N50°W-striking, vertical strike-slip faults following 120 m of sea-level rise. (B) Normal (blue), shear (green), and Coulomb stress (red) on the actual San Andreas fault plane whose surface trace is shown as bold black in (A). Modified from Luttrell and Sandwell (2010).

3.2 Consequences of recent climate change

Since the 1800s, human activities have been the main driver of climate change (IPCC, 2021). As modern Earth's climate warms at unprecedented rates, it promotes faster melting of the polar ice caps (The IMBIE team, 2018; 2020; Hugonnet et al., 2021), thereby raising sea levels (e.g. Frederikse et. al, 2020). It also accelerates global and regional trends in precipitation and water runoff and enhances regional floods and droughts (e.g., Dai, 2016; Gudmundsson et al., 2019). Moreover, groundwater, which serves as a water-shortage buffer, is subject to major fluctuations and often rapid depletion in some regions (e.g., Green et al., 2011). Particularly, groundwater extraction in coastal regions can cause subsidence that adds to relative sea-level rise and increases the risk of floods (e.g., Shirzaei et al., 2021; Tay et al., 2022; Wu et al., 2022). Accelerating changes in the global water distribution and rising temperatures, occurring over timescales ranging from months to centuries, cause the Earth to move through (visco-)elastic, poroelastic and/or thermoelastic deformation, inducing stresses that may modulate tectonic seismicity and possibly reactivate formerly stable faults.

In polar regions, glaciers and ice sheets are undergoing massive ice loss on timescales similar to the seismic cycle, with meters per year thinning in regions of ablation (Shepherd et al., 2012; Mouginot et al., 2019). Glacier surges, during which ice flow velocities transiently increase by orders of magnitude, can abruptly modify the distribution of ice load through catastrophic glacier

collapse (Kääb et al., 2018). In addition, several regions such as Patagonia (Dietrich et al., 2010), Alaska (Larsen et al., 2005), the Alps (Barletta et al., 2006), and Greenland (Adhikari et al., 2021), have been impacted by rapid GIA as a result of glacial unloading following the end of the Little Ice Age, a period of regional cooling from the early 14th century to the mid-19th century during which glaciers and ice-sheets expanded. Present-day ice mass loss induces an instantaneous elastic response of the solid Earth, while past ice loss contributes a prolonged viscoelastic response. These two responses may act simultaneously and produce among today's fastest surface uplift rates on Earth exceeding 30 mm/yr, and are also associated with mm/yr horizontal deformation (Hu and Freymueller, 2019; Adhikari et al., 2021). This combined glacial unloading effect can influence seismicity in volcanic (e.g. Sigmundsson et al., 2010), and tectonic dip-slip and strike-slip settings (Sauber et al., 2000, 2021; Rollins et al., 2021). Rollins et al. (2021) illustrate the viscoelastic stress changes associated with a scenario of 1 m/yr glacial unloading over 200 years, alongside a vertical strike-slip fault. Rapid GIA acts to unclamp the fault, promoting fault failure, and the Coulomb stress (Figure 4) amplitude reaches 0.5 MPa with an asymmetrical distribution caused by the unloading location with respect to the fault (Figure 8A).

A particularly interesting region to investigate the impact of present-day ice retreat, thinning surges and GIA following the Little Ice Age is Southern Alaska, a rapidly deforming and seismically active setting with thrust and strike-slip faults. In the Bering glacier region, Sauber and Molnia (2004) found an increase/decrease in the seismicity rate associated with ice thinning/thickening over the 1995-2000 period, modulated by glacier surges. Similarly, Sauber and Ruppert (2008) suggest that the rapid ice wastage between 2002 and 2006 in the Icy Bay may have affected seismicity rates in the area. At longer timescales, Rollins et al. (2021) show that rapid GIA following the thinning of the Bay Icefield since 1770, and elsewhere in southeast Alaska since 1900, likely promoted Coulomb stress at the location of the 1958 Mw 7.8 Fairweather Fault earthquake and of at least 23 of 30 known Mw$\geq$5.0 earthquakes in southeast Alaska (Figure 8B).

In other polar regions, where tectonic deformation is occurring at much lower rates, correlations between recent ice melting and seismic activity are more difficult to establish. In Greenland, earthquakes mainly occur along continental margins, which coincide with the ice sheet margin and where most of the recent ice melting occurs. While Olivieri and Spada (2015) could not find a clear correlation between seismicity and recent glacial unloading, they interestingly suggest that GIA in response to the melting of the late-Pleistocene ice sheet may have promoted regional moderate-size crustal earthquakes, whereas recent ice melting may be associated with local shallower and smaller events. However, the link between seismicity and recent ice melting may be more complex. Indeed, Lough et al. (2018) reported 27 extensional shallow to mid-crustal intraplate earthquakes in East Antarctica that occurred in 2009, a region with no significant recent changes in ice mass (Whitehouse et al., 2012; Martin-Espanol et al., 2017), and suggested the influence of pre-existing tectonic weakness or subglacial hydrological processes on the seismic activity.

Recent climate change also impacts groundwater storage through an increase in frequency and intensity of extreme weather events, such as droughts, as well as anthropogenic activities (IPCC, 2022). Sustained aquifer depletion over years to centuries can cause the Earth's surface to subside by up to tens of centimeters per year and will also impact the regional stress field and potentially influence seismic activity. In California, decades of continual groundwater pumping have already resulted in tens of meters of water level drop and meters of irreversible land subsidence (Galloway et al., 1999), at rates modulated by climate forcing with more groundwater used during dry periods related to the evolving El Nino/La Nina cycles (e.g., Faunt et al., 2016). The Central Valley, which is surrounded by active faults and has experienced multiannual periods of drought, has been particularly intensively studied for changes in groundwater, surface deformation, and Coulomb stress on nearby faults. GNSS (Amos et al., 2014; Argus et al., 2017) and InSAR (Smith et al., 2017; Ojha et al., 2019) observations indicate subsidence rates ranging from a few mm/yr to 0.3 m/yr, inducing Coulomb stress changes of a few Pa to a few kPa in the crust (Johnson et al., 2017a,b; Carlson et al., 2020). Moreover, Lundgren et al. (2022) investigate viscoelastic effects

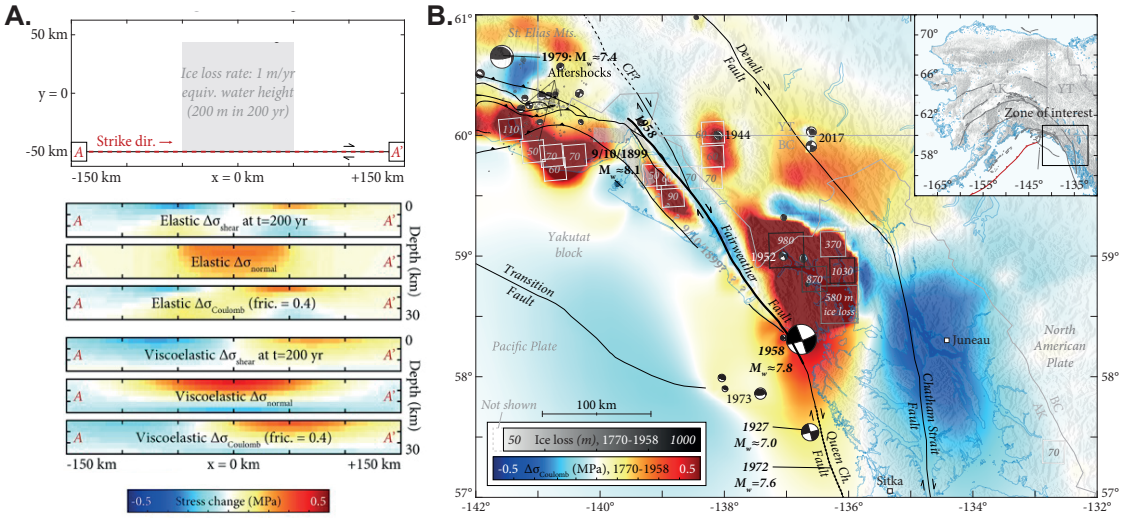

Figure 8: (A) Elastic and viscoelastic effect of cumulative 200-year shear, normal and Coulomb stress changes on a vertical right-lateral strike-slip fault caused by a constant ice unloading rate of 1 m/yr equivalent water height (gray) for a fault located at the edge of the 100 km by 100 km zone of unloading. Stresses are positive for unclamping. (B) Coulomb stress changes as of 1958 at 10 km depth induced by rapid GIA since 1770 in Southern Alaska. Ice mass loss in meters of equivalent water height is shown by gray squares. Mw $\geq$ 5.0 earthquakes occur preferably in regions where rapid-GIA driven Coulomb stress promotes failure. Modified after Rollins et al. (2021).

accompanying groundwater unloading using a 150 years historical groundwater change record. They show that the associated cumulative Coulomb stress change on the San Andreas fault is of the order of 0.01-0.02 MPa, comparable to Coulomb stress increases triggering seismicity following large earthquakes (Stein, 1999). Kundu et al. (2015) and Kundu et al. (2019) argue that stress changes due to long-term groundwater extraction and hydrological unloading substantially contributed to the stress levels at the times of the 2015 M7.8 Gorkha earthquake and 2017 M7.3 Iran–Iraq border earthquake. While these studies show clear groundwater-loss induced strain and stress changes, assessing the impact on seismicity or the timing of individual large earthquakes is not straightforward at these longer time scales.

Young et al. (2021) document vertical uplift and horizontal extension around Great Salt Lake during the 2012–2016 drought, showing that in addition to the load reduction associated with lake-level drop, additional water storage loss must have occurred in surrounding aquifers. They also suggest that earthquakes within the region affected by Great Salt Lake and surrounding groundwater occur preferentially during dry multi-year periods and the earthquake rate appears anti-correlated with the lake elevation rate. In turn, earthquakes outside the load region exhibit no relationship.

Other examples of earthquake triggering by long-term groundwater loss include the 2011 Lorca earthquake in Spain (Gonzalez et al., 2012), earthquake swarms near the Dead Sea Fault (Wetzler et al., 2019), and the 2016 Petermann Ranges and other shallow intraplate earthquakes in central Australia (Wang et al., 2019). These earthquakes occurred at very shallow depths, in regions where Coulomb stress induced by long-term fluctuations in nearby groundwater promoted failure, providing insights into poroelastic processes that could modify seismic hazard in regions where large aquifer depletion occurs.

In contrast, temperature changes of a few degrees over the next century, as projected by climate models (IPCC, 2021), are expected to only induce negligible thermoelastic deformation and stress. These longer-term changes are indeed substantially smaller than annual temperature variations of a few tens of degrees which result in deformation of a few mm (Dong et al. 2002; Xu et al., 2017) and stress of a few hundred Pa (Figure 9; Johnson et al., 2017b). Similarly, the changes in stressing rate on near-coastal faults due to the anticipated acceleration in sea level rise by several mm/yr (IPCC, 2021), are unlikely to lead to a notable rise in earthquake occurrences or hazards.

3.3 Seasonal hydrological and atmospheric loads

The large-scale seasonal water cycle and associated mass redistribution couple with the solid Earth and cause periodic loading strain and stress variations. The hydrologically induced loading stress change may modulate seismicity, if they are large enough in amplitude and consistent with the background tectonic stress in orientation. In the Nepal Himalaya, Bettinelli et al. (2008) reported that the seasonal summer monsoon produces ∼2-4 kPa loading stress change on the Main Himalayan Thrust zone, and the seismicity rate in winter is twice that in the summer at all magnitudes above the detection threshold ($M > 2.2$). In Japan, Heki (2003) showed that the snow load on the western flank of the backbone mountain ranges causes a few kPa stress change, and the spring thaw decreases compressional stress and correlates with an increase in the number of $M \geq 7$ earthquakes. In California, Johnson et al. (2017a and 2017b) modeled the seasonal loading strain and stress changes by annual snow and rainwater and showed that 1-5 kPa hydrologically induced loading stress changes are correlated with a ∼10% increase in seismicity when the stress conditions favor slip on faults. This correlation also holds for damaging $M>5.5$ earthquakes in catalogs reaching back to 1781 (Johnson et al., 2017a). Horizontal GNSS displacements have also been used to estimate seasonal strain variations and to discuss their potential association with seismicity in California (e.g., Kreemer and Zaliapin, 2018; Kim et al., 2021b). Kreemer and Zaliapin (2018) proposed that hydrologically induced seasonal strain may cause a larger stress release in an earthquake and fewer aftershocks. In the intra-continental New Madrid seismic zone, Craig et al (2017) identified annual and multi-annual variations in microseismicity rates ($M \leq 2.3$) that coincide with stress variations driven by elastic hydrological loading. In southern Alaska, Johnson et al. (2020) analyzed the shallow seismicity (< 40 km) and found a seasonality with more events in winter, which correlates with ∼10 kPa seasonal loading stress changes by surface snow and rainwater. Xue et al. (2020) compared seasonal seismicity rate variations and water level changes of Lake Victoria and surrounding rift lakes in the western branch of the East African Rift Valley, and suggested the seasonal 0.2-0.8 kPa Coulomb stress changes due to lake water loading modulate seasonal seismicity rate variation. In western Taiwan, Hsu et al. (2021) reported a seasonal pattern with a higher seismicity rate from February to April and a lower rate from July to September, which is associated with annual water storage unloading.

In addition to hydrological loading by terrestrial water movement, atmosphere pressure loading (e.g., van Dam et al., 1994), solid Earth tides (e.g., Wahr, 1995), tidal and nontidal ocean loading (e.g., Agnew, 2015), and thermoelastic strain (e.g., Dong et al., 2002) of the crust all produce elastic strain and stress on the surface and in the interior of the Earth. Gao et al. (2000) propose that seasonal changes in atmospheric pressure of ∼2 kPa modulated seismicity in geothermal and volcanic regions of California over a five-year period following the 1992 Landers earthquake. Johnson et al. (2017b) modeled and compared seasonal stress changes on the faults in California from several sources, concluding that in most locations the hydrological water loading is the largest source of seasonal stress variation, followed by contributions from atmospheric and thermoelastic stress perturbations (Figure 9B).

Besides analyzing the statistical correlation between environmentally induced stress changes and seismicity-rate variations, research was also carried out to investigate the possible triggering relationship with individual earthquakes. In California, Kraner et al. (2018) used horizontal

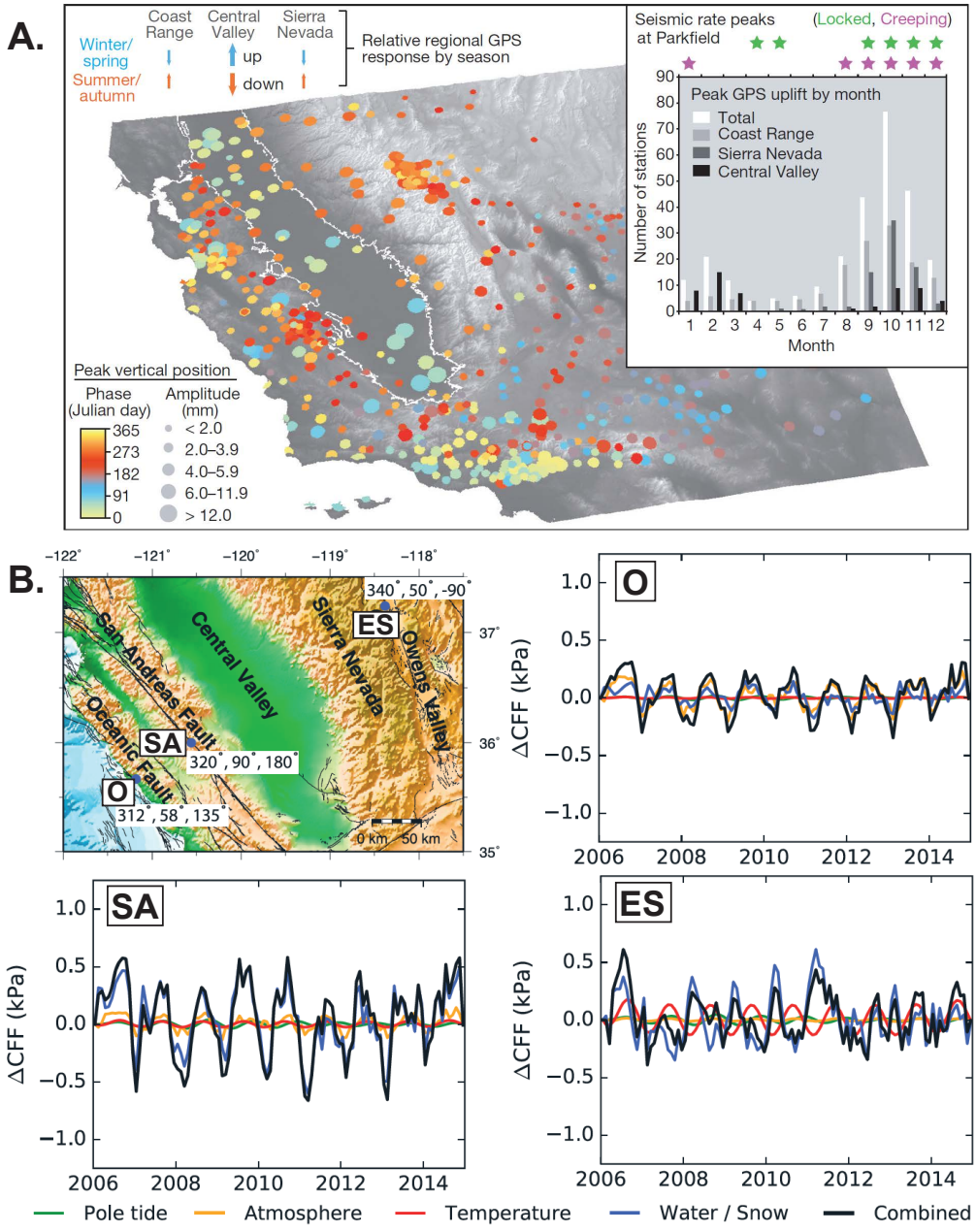

Figure 9: (A) Phase and amplitude of peak GNSS vertical position in California. The histograms in the inset show the results of peak GNSS uplift in the Coast Range, Sierra Nevada and Central Valley, respectively. The comparison with seismicity rate variation indicates that both the locked and creeping sections of the San Andreas Fault at Parkfield exhibit more events in dry later summer and autumn, corresponding to the fault unclamping caused by the unloading of seasonal terrestrial water mass. Modified from Amos et al. (2014). (B) Coulomb stress changes (with a friction coefficient $\mu = 0.4$) at three locations of three faults (O. Oceanic Fault; SA. central San Andreas Fault; ES. eastern Sierra range front normal fault) from different sources of periodic stress. Strike, dip, and rake directions of the corresponding receiver fault are labeled at each location. Modified from Johnson et al. (2017b).

GNSS time series to calculate the strain and stress changes in the northern San Francisco Bay Area and found the 2014 M6.0 South Napa earthquake occurred during a period with peak seasonal Coulomb stress. Using a similar method, Kim et al. (2021a) reported that the 2019 Ridgecrest earthquake sequence took place at a time with higher seasonal stress. Both studies suggested the possible earthquake triggering from non-tectonic seasonal loading in California (Johnson et al., 2017a). Hu et al. (2021) modeled the stress perturbations by hydrological and industrial loads in the Salt Lake City region and assessed the possible correlation with the 2020 M5.7 Magna earthquake, but no definite link was found. Yao et al. (2022) reported that the 2019 M4.0 Ohio earthquake occurred when water level of Lake Erie was high. They calculated the elastic Coulomb stress change by lake-water loading, but a clear connection could not be found because of the uncertainty of the frictional coefficient in the region. It is generally difficult to confidently link modest seasonal stress changes with the occurrence of single large earthquakes, as it is not known when those events would have occurred without such perturbations.

Some studies also focused on poroelastic stress changes due to subsurface groundwater and aquifer pressure variations and their role in annual seismicity modulation. Kraft et al. (2006) identified a higher seismicity rate in summer coinciding with the increase of precipitation and groundwater level in the region of Mt. Hochstaufen, Germany. At the Long Valley Caldera, California, Montgomery-Brown et al. (2019) showed the shallow seismicity rate significantly increased during the wet snowmelt season compared with the dry season and concluded that groundwater recharge and pore fluid pressure accelerated earthquake occurrences. Christiansen et al. (2007) statistically analyzed earthquake records of the San Andreas Fault near Parkfield, California, identified an annual period in the creeping section and a semiannual period in the locked section of the fault, and suggested pore-pressure diffusion may play a role in the observed modulation. Seasonal seismicity at some volcanic centers of the western U.S. was also discovered and was inferred to be associated with pore-fluid pressure changes due to groundwater recharge (Saar and Manga, 2003; Christiansen et al., 2005).

3.4 "Earthquake Weather"

Short-term weather events involve rapid spatiotemporal variations in atmospheric pressure, temperature and precipitation. Atmospheric pressure changes produce relatively modest surface loads, but they can approach 10 kPa during the passage of great tropical cyclones (hurricanes and typhoons). Liu et al. (2009) propose that transient strain signals during the passage of eleven great typhoons in Taiwan reveal the occurrence of aseismic slip events on buried faults triggered by the associated low atmospheric-pressure transients. Hsu et al. (2015) considered strain from precipitation loading in addition to barometric pressure to find that much of the strain signal attributed to triggered slow slip events by Liu et al. (2009) can be explained by hydrological processes. However, some of the strain events associated with typhoons still appear to require a tectonic explanation (Hsu et al., 2015). Zhai et al. (2021) argue that the seismicity rate in an ongoing earthquake swarm in northeast Taiwan in August of 2009 was transiently subdued by the local reduction of atmospheric pressure by almost 6 kPa associated with the passage of typhoon Morakot's eye. In 2017, a burst of seismicity in the aftershock zone of the M 5.7 Virginia earthquake in the eastern U.S. occurred just when atmospheric pressure dropped during the passage of Hurricane Irene 3-5 days following the mainshock, suggesting a causal relationship (Meng et al., 2018). While only a few cases of earthquake or slow-slip triggering by short-term atmospheric pressure changes have been reported, the fact that transient stress changes in the crust from such events are comparable to those leading to seismicity rate changes due to other forcings suggests that this is likely a real phenomenon.

In addition to extreme storm events and associated atmospheric pressure changes, there are also daily temperature and atmospheric pressure cycles. Diurnal pressure variations are maximum near the equator, where the average amplitude reaches 300 Pa. Such atmospheric tides have been shown to modulate the motion of shallow slow-moving landslides (Schulz et al., 2009). However,

daily modulation of seismicity has not been documented so far and is challenged by periods very close to those of the soli-lunar tides and the need to separate any subtle seismicity-rate changes from the effect of daily variations in seismic noise and thus network sensitivity.

Great cyclones also represent extreme precipitation and hydrological loading events, and the largest storms with m-level precipitation, such as Hurricane Harvey in Texas in 2017 (Milliner et al., 2018) and typhoon Hagibis in Japan in 2018 (Zhan et al., 2021), led to multi-day subsidence of the Earth's surface by up to 20 mm, as measured by GNSS. Heki and Arief (2022) document similar multi-day subsidence events of 10-20 mm caused by loads in flooded areas during four large tropical rainstorms in Japan. Depending on the spatial extent of such load changes, storm-related stress changes at seismogenic depth may reach several-kPa; however, no earthquake triggering has been recognized in these cases. Typhoon Morakot in Taiwan produced up to 3 m of rainfall over the course of 5 days. The impact of the storm on the seismic network and noise levels made it impossible to resolve significant changes in seismicity during and in the days following the storm (Zhai et al., 2021). More comprehensive analysis is needed to properly assess the possible linkage of hydrological load transients of a few days and crustal seismicity.

In areas dominated by highly fractured rock in the uppermost crust, such as karst geology marked by caves and open fracture systems, individual rain storms appear to be capable of triggering earthquakes (e.g., Hainzl et al. 2006; Rigo et al. 2008; Husen et al. 2007; Chmiel et al., 2022). In these cases, the delay between peak rainfall and seismicity-rate increases can be just a few hours or days. Montgomery-Brown et al. (2019) document seismic swarm activity in the upper few km of the crust near Long Valley Caldera in California, which follows stream-flow peaks with an average delay of 3 to 4 weeks (Figure 10). Silverii et al. (2020) show that this seismic activity is also correlated with horizontal displacement transients at nearby GNSS stations, which can be explained with a poroelastic model of a distributed pressure source. This suggests that pore pressure diffusion through fractured rock in the area drives both the shallow seismic swarms and the GNSS-measured deformation. These cases of quite rapid activation of shallow seismicity suggest effective triggering by rapidly increasing fluid pressure and extension in a highly permeable upper crust and/or fluid-pressure increases in saturated rocks due to near-surface hydrological loading (e.g., Miller, 2008; d'Agostino et al., 2018; Chmiel et al., 2022). Thus, the local geology and permeability structure of an area appear to be important factors that determine the susceptibility to weather-induced earthquake triggering by elastic surface loading, rapid pore-pressure diffusion, and/or poroelastic strain.

Great storms may leave a more enduring change in stress and seismicity through the enormous amount of erosion and sediment transport they cause. Steer et al. (2020) note an increase of shallow (<15 km) earthquakes in the years following the August 2009 typhoon Morakot, which they attribute to crustal unloading due to rapid sediment export after the storm's passage. Zhai et al. (2021) also infer a rise in background seismicity rate in the year following the event. However, Hsu et al. (2021) note that these years of enhanced seismicity also correlate with a period of low water storage in south Taiwan, thus suggesting an example of multi-year hydrological load triggering that is unrelated to the typhoon.

As global weather becomes more energetic and extreme storm events more common (e.g., Otto, 2017), we can expect to see more cases of weather-triggered seismicity, especially in areas dominated by highly fractured and permeable rocks and regions exposed to extreme tropical storm systems and associated catastrophic rainfalls. Nonetheless, we don't expect "weather earthquakes" to become a significant source of natural hazard, given the relatively modest stress and pressure changes and earthquake magnitudes associated with the documented cases of triggering by individual weather events.

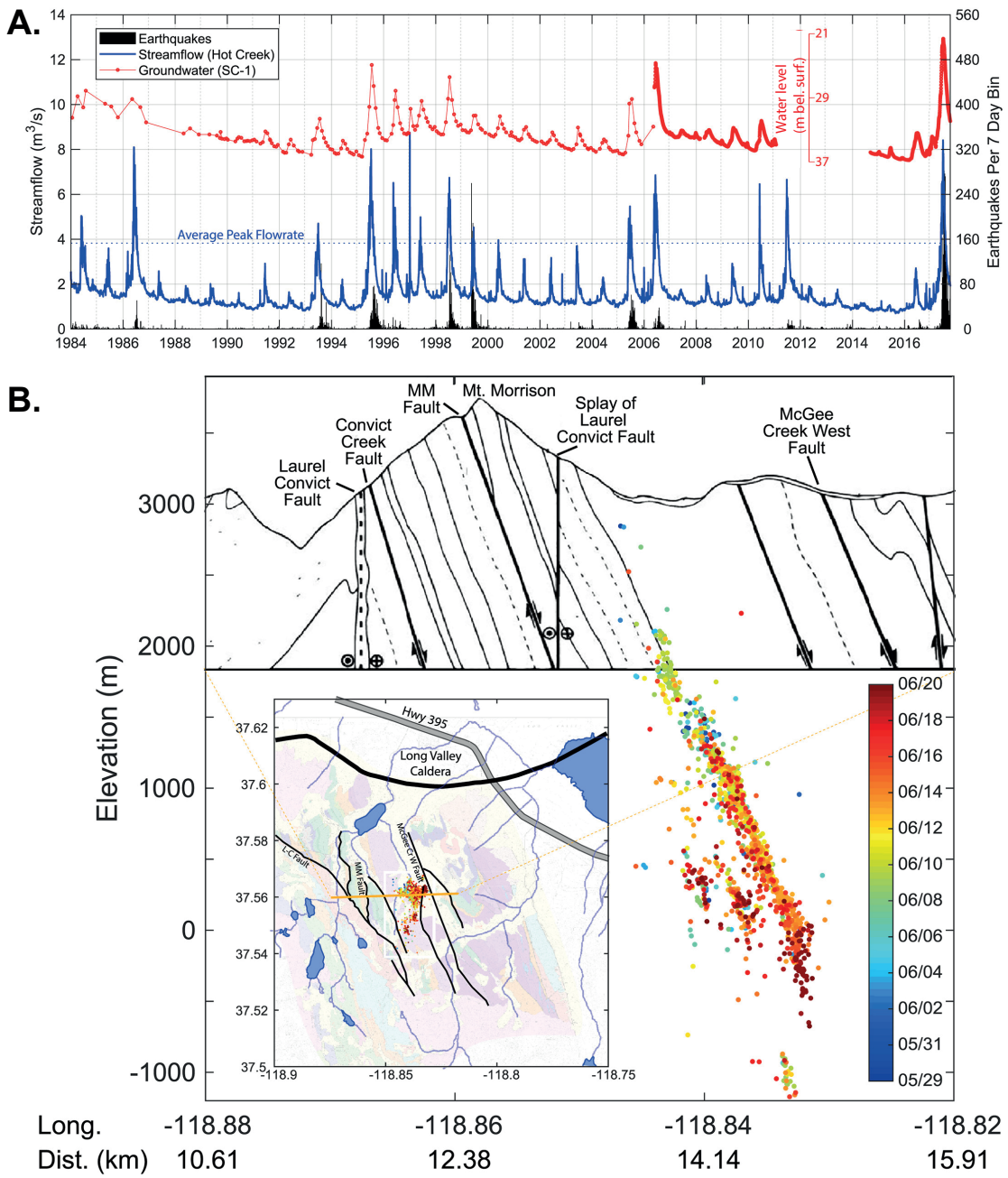

Figure 10: Rainfall-triggered swarm seismicity south of Long Valley Caldera, California. (A) 35-year time series of streamflow in a nearby creek (blue line), local groundwater level (red line), and weekly earthquake counts (black bars) in the seismic swarm area. (B) Four weeks of seismicity in June 2017, color-coded by time and superimposed on a simplified geologic cross section (orange line in inset map). The swarm propagated downward along the dipping bedrock bedding contacts and fractures. Modified from Montgomery-Brown et al. (2019).

4 Lessons Learned from Climate-driven Deformation and Seismicity

4.1 Probing the Earth's constitutive properties using climate-driven deformation

Interactions between climate and solid-Earth deformation include multiple forcings, such as heavy rain and cyclones (< days), annual and multi-year hydrologic loading cycles (years to decades), as well as unloading due to recent ice melting (years–decades), since the little ice age (250 years) and since the last glacial maximum (25,000 years). These interactions involve various physical processes acting over a range of spatial and temporal scales. The deformational response of the solid Earth to these forcings depends on the constitutive properties of the crust and mantle, that is its rheological structure.

Deformation caused by changes in surface loading, which dominates this interplay, has been a key observation to probe the Earth's mantle rheology (Figure 11A). Mantle viscosity has been inferred from observations related to glacial isostatic adjustment (e.g., Haskell, 1935; Peltier & Andrews, 1976; Mitrovica & Forte, 2004; Lau et al., 2016) while rheology of the upper mantle has been constrained using geodetic measurements following lake drainage (e.g., Bills et al., 2007; Austermann et al., 2020) (Figure 11B). The time-dependent response of the Earth's mantle to stresses induced by surface loading has been shown to progress through instantaneous elastic strain, transient creep during which viscosity rapidly increases, to a steady-state viscous regime. This is supported by laboratory experiments investigating deformation of crystalline aggregates that have yielded constitutive laws allowing extrapolation to mantle conditions (e.g., Hirth and Kohlstedt, 2003; Hansen et al., 2011). However, the majority of climate-driven mantle rheology studies have focused on mantle elasticity and steady-state creep through observations at short and very long timescales, respectively. Therefore, the mantle is often described as a Maxwell body, characterized by a shear modulus for the elastic strain and a linear viscosity for the long-term strain rate.

However, over the past decades, emerging geodetic technologies and continuously growing spatio-temporal coverage have provided new opportunities to probe the solid Earth's rheology using its response to changes in surface loading. It is becoming increasingly clear that the Maxwell framework, with a single viscosity, is inadequate for capturing processes at intermediate time scales such as recent ice melting (years to decades; Nield et al., 2014) or since the Little Ice Age (250 years). The inference of time- and stress-dependent viscosity is also supported by studies of postseismic relaxation of the mantle (e.g., Bürgmann and Dresen, 2008). Indeed, the viscoelastic relaxation of coseismic stresses in the lower crust and upper mantle with multiple relaxation times and/or power-law rheologies, better explains the time series of postseismic deformation (e.g., Pollitz et al., 2003; Freed and Bürgmann, 2004; Trubienko et al., 2014). At the annual timescale, Chanard et al. (2018b) demonstrated that Earth's response to seasonal surface loading, which is primarily driven by continental hydrology, can be used to constrain a lower bound on the globally averaged transient viscoelastic properties of the upper mantle using an approach relying on multiple geodetic techniques. Pollitz et al. (2013) also explored phase delays in the deformational response to surface loading due to the viscoelastic Earth structure. These studies imply that long geodetic time series of hydrological load deformation could be used to obtain new rheological constraints over a wider range of periods. Reconciling observations at multiple timescales will require a fully consistent rheological model (Lau and Holtzmann, 2019; Lau et al., 2021).

Variations in groundwater storage and associated poroelastic deformation can also be used to probe the mechanical properties of the Earth's shallow subsurface (e.g., Larochelle et al., 2022). Moreover, investigating the rheological processes behind irreversible aquifer compaction and depletion offers an opportunity to better understand the inner workings of groundwater systems,

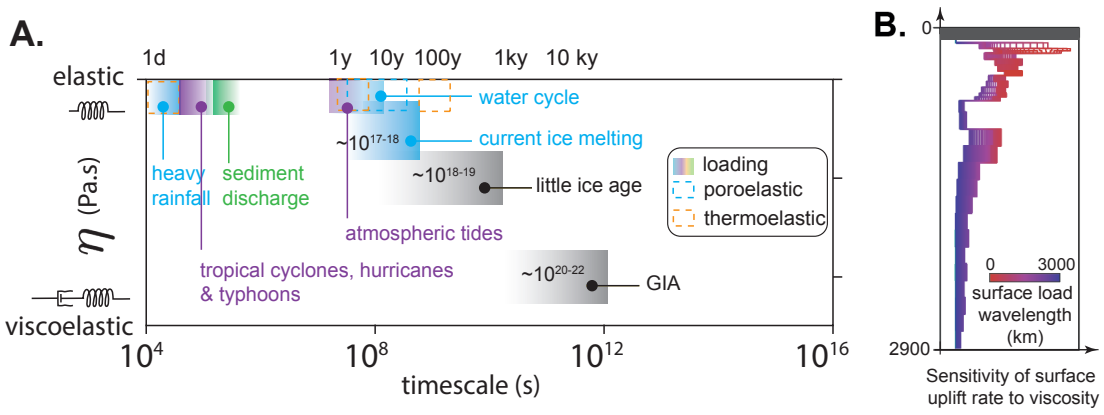

Figure 11: (A) Schematic illustration of climate-driven processes used to probe Earth's rheology. (B) Sensitivity of surface uplift rates to viscosity of the Earth interior as a function of surface load spatial wavelength (λ) (Chanard et al., 2018b).

necessary to ensure sustainability of freshwater resources (Smith et al., 2017; Ojha et al., 2018; Chaussard and Farr, 2019). While the Earth's response to periodic loading processes has been theoretically and numerically investigated, the role of climate-driven processes generating eigenstrain in the shallow subsurface, including fluctuations in groundwater pressure or near-surface temperature, in earthquake modulation or triggering remains poorly known. Stresses associated with seasonal eigenstrain and variations of mechanical properties at short wavelengths that are likely to occur at shallow depths, can reach up to a few kPa at a few km depth (Ben-Zion & Allam, 2013), comparable to those induced by annual hydrological loading. Interestingly, these stresses may localize across fault damage zones where detailed seismic imaging shows strong variations in seismic velocities (up to 50%) relative to the surrounding host rock in the crust at 3-5 km depth (Ben-Zion et al. 2003; Allam et al. 2014; Qin et al. 2018). Carefully conducted field studies combined with advances in modeling approaches are needed to better understand the role of poroelastic and thermoelastic processes and associated constitutive properties of the shallow crust in the Earth's response to climatic variations. The use of more advanced physical models of Earth's deformation and stress in response to climate and weather changes over a wide range of spatial and temporal scales will also improve our ability to link these processes to the occurrence of earthquakes.

4.2 Insights on frictional fault properties and state of stress in the Earth from periodic climate forcing

Just as the Earth's deformational response to external forcings reveals new insights about its constitutive properties, the occurrence of earthquakes or slow slip events in response to these forcings can inform us about the environment and frictional mechanics of faults. Similar to solid Earth and ocean tides (Heaton 1982; Vidale et al., 1998), stresses resulting from climate forcing, of comparable amplitude, may not be sufficient to cause earthquakes. Faults may need to be critically stressed from long-term tectonic loading (Figure 12A), as supported by laboratory experiments (Chanard et al., 2019; Noël et al., 2019), and/or combined with favorable conditions including low-angle fault orientations and shallow depths (Cochran et al., 2004), resonant fault-frictional properties (Perfettini et al., 2001; Lowry, 2006; Senopati et al., 2022), or high pore pressure in the fault zone (Bettinelli et al., 2008). Considering natural and laboratory observations, there is growing appreciation for the fact that faults' response to small climate-driven stress perturbations may indicate favorable frictional properties and conditions for rupture (Figure 12A).

While Coulomb failure stress is often invoked to explain interactions between periodic loading

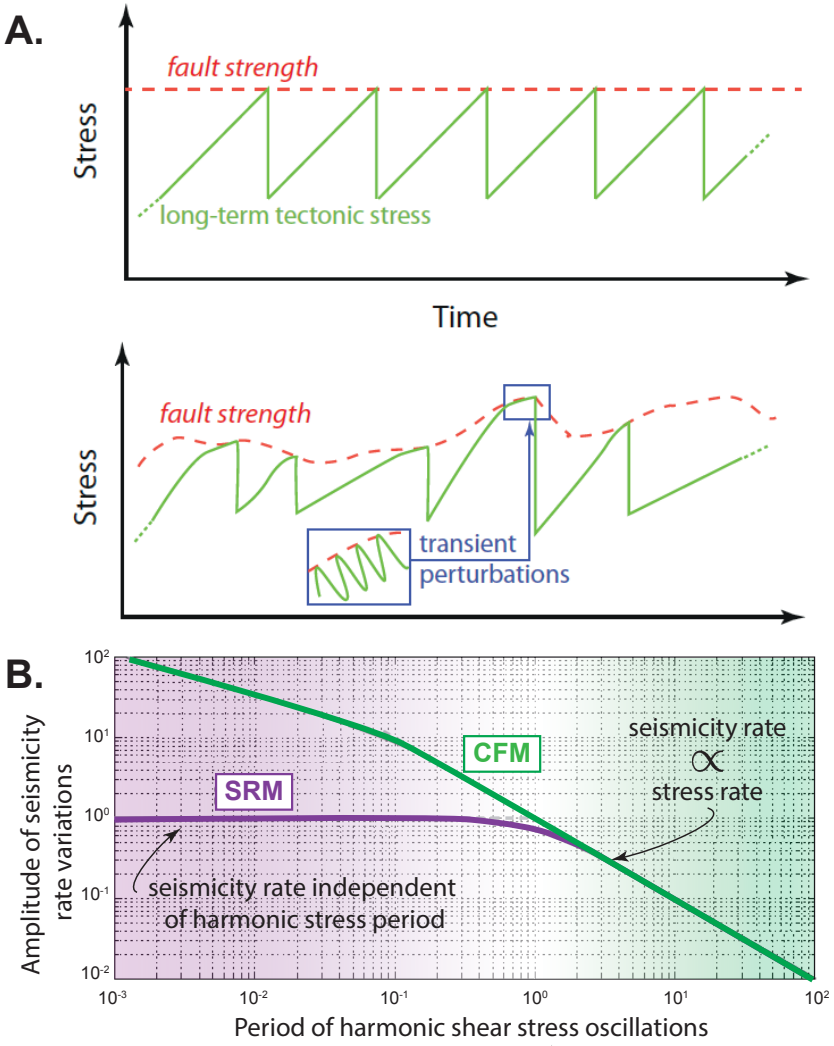

Figure 12: (A) Schematic illustrating the state of stress and strength on a fault with a constant loading rate, stress drop, and strength from which perfectly periodic failure results (top) and with variable loading rate, stress drop, and strength in a more realistic scenario (bottom). In a natural system, a fault is stressed by external perturbations, including climatic forcings, in addition to long-term tectonic stress. Transient stress, even small, may initiate failure of a fault in a critical state of stress and detailed observations of triggered small earthquakes may provide information on state of stress and frictional properties of faults. (B) Amplitude of seismicity-rate variations as a function of the shear stress oscillation period, according to the numerical (black) or asymptotic (gray) solutions for the Coulomb failure model (CFM) and spring-slider rate-and-state model (SRM). Figure modified from Ader et al. (2014).

and seismicity (e.g. , Johnson et al., 2017a; Scholz et al., 2019), some laboratory and natural observations suggest a time-dependent failure process (e.g., Beeler and Lockner, 2003). Models developed to explain these observations include rate-and-state spring-slider systems to simulate earthquake nucleation under periodic loading (Ader et al., 2014; Heimisson & Segall, 2018; Heimisson & Avouac, 2020) or Burridge-Knopoff models (e.g., Pétrélis et al., 2021). More realistic descriptions such as 2-D faults (Perfettini et al., 2003; Ader et al., 2014) or even a 3-D interacting fault population in a rate-and-state framework under periodic loading (Dublanchet, 2022) confirm prior theoretical results with numerical simulations. These models suggest that seismicity rate correlates with stress amplitude when the loading period is short compared to the characteristic nucleation time but correlates with stressing rate for longer periods (Figure 12B). Models also suggest that the highest correlation should occur at periodic loading near the characteristic nucleation time. Perfettini et al. (2001) showed a potential fault-slip resonance, invoking enhanced modulation of a spring-slider system with rate-weakening rheology subject to periodic loading near a critical period. The frequency-dependent modulation of earthquakes inferred from the experimental results and model predictions has been invoked to explain why there is seasonal modulation in areas that lack evidence of modulation by the higher-frequency tides, suggesting that the earthquake nucleation time is close to a year (e.g., Beeler and Lockner, 2003; Ader and Avouac, 2013; Johnson et al., 2017a). Furthermore, by coupling the amplitude and frequency of periodic loading to mechanical parameters such as stress drop and frictional fault properties, some of these models provide a mechanical framework to further our understanding of periodic seismic modulation.

5 Summary and Future Opportunities

In this chapter, we review the coupling effects of the solid Earth with climate and weather systems over a wide range of spatiotemporal scales. Large ice-sheet and lake-load changes, such as those associated with the Last Glacial Maximum and glacial isostatic adjustment, can trigger substantial earthquakes. More modest forcings due to climate processes at multi-annual time scales may result in more subtle strain and seismicity responses. Annual hydrological loading and other seasonal forcings produce geodetically measurable, periodic deformation cycles and can significantly modulate seismicity on suitably oriented faults. In a few cases, even atmospheric pressure, hydrological surface loads, and/or subsurface fluid pressure transients associated with short-term weather events can affect earthquake occurrences. Most climate-driven stress and strain changes in the Earth are small and careful mechanical modeling and statistical analysis are required to discern their effect on earthquake occurrence. While there is solid evidence for climate-driven modulation of seismicity, the impact of ongoing climate change and sea level rise caused by anthropogenic emissions on short- or long-term seismic hazard is probably modest.

Future studies are recommended to investigate the contributions from multiple processes, including atmospheric and hydrological surface loads as well as poroelastic and thermoelastic strain. These processes need to be carefully modeled to develop a comprehensive and quantitative understanding of the climate-driven stress tensor changes and associated solid-Earth deformation and seismicity. We should seek evidence for, and causes of, variable seismicity modulation in different tectonic environments. We can also further improve knowledge of fault-frictional properties based on observations of perturbed seismicity over a range of forcing periods. Finally, it may be possible to determine viscous rheological properties in the lower crust and upper mantle from geodetic observations of the spatio-temporal response of the Earth to periodic loads.

Acknowledgments: We thank everybody who provided figures and/or helpful discussions and thoughtful comments during the preparation of this review, including Karen Lutrell, Emily Montgomery-Brown, Chris Rollins, Holger Steffen, Rebekka Steffen, Manoochehr Shirzaei, Patrick Wu, and Timothy Craig. Francesca Silverii and Corné Kreemer provided helpful review comments. We also acknowledge support from NASA's Earth Surface and Interior program and CNES's TOSCA program (HydroGeo project).

Chapter References:

Aagaard, B., M. Knepley, and C. Williams. (2017), PyLith v2. 2.1 Davis, CA: Computational Infrastructure of Geodynamics.

Adams, K. D., & Bills, B. G. (2016). Isostatic rebound and palinspastic restoration of the Bonneville and Provo shorelines in the Bonneville basin, UT, NV, and ID. In Developments in Earth Surface Processes (Vol. 20, pp. 145-164). Elsevier.

Ader, T. J., & Avouac, J. P. (2013). Detecting periodicities and declustering in earthquake catalogs using the Schuster spectrum, application to Himalayan seismicity. Earth and Planetary Science Letters, 377, 97-105.

Ader T.J., Lapusta N., Avouac J.-P., Ampuero J.-P., 2014. Response of rate-and-state seismogenic faults to harmonic shear-stress perturbations, Geophys. J. Int., 198(1)

Adhikari, S., Ivins, E. R., & Larour, E. (2016). ISSM-SESAW v1.0: Mesh-based computation of gravitationally consistent sea-level and geodetic signatures caused by cryosphere and climate driven mass change. Geoscientific Model Development, 9(3), 1087– 1109. https://doi.org/10.5194/gmd-9-1087-2016

Adhikari, S., Milne, G. A., Caron, L., Khan, S. A., Kjeldsen, K. K., Nilsson, J., ... & Ivins, E. R. (2021). Decadal to centennial timescale mantle viscosity inferred from modern crustal uplift rates in Greenland. Geophysical Research Letters, 48(19), e2021GL094040.

Agnew, D. C. (1997). NLOADF: a program for computing ocean-tide loading, J. Geophys. Res.,102, 5109-5110.

Agnew, D. (2015). Earth tides. In Treatise on Geophysics (pp. 151– 178). Amsterdam: Elsevier. https://doi.org/10.1016/B978-0-444-53802-4.00058-0

Allam, A. A., Ben-Zion, Y., & Peng, Z. (2014). Seismic imaging of a bimaterial interface along the Hayward fault, CA, with fault zone head waves and direct P arrivals. Pure and Applied Geophysics, 171(11), 2993-3011.

Altamimi, Z., Rebischung, P., Collilieux, X., Métivier, L., & Chanard, K. (2023). ITRF2020: An augmented reference frame refining the modeling of nonlinear station motions. Journal of Geodesy, 97(5), 47.

Altamimi, Z., Rebischung, P., Métivier, L., & Collilieux, X. (2016). ITRF2014: A new release of the International Terrestrial Reference Frame modeling nonlinear station motions. Journal of geophysical research: solid earth, 121(8), 6109-6131.

Amelung, F., D. L. Galloway, J. W. Bell, H. A. Zebker, and R. J. Laczniak (1999), Sensing the ups and downs of Las Vegas-InSAR reveals structural control of land subsidence and aquifer-system deformation, Geology, 27, 483– 486.

Amos, C. B., Audet, P., Hammond, W. C., Bürgmann, R., Johanson, I. A., & Blewitt, G. (2014). Uplift and seismicity driven by groundwater depletion in central California. Nature, 509(7501), 483-486.

Argus, D. F., Y. Fu, and F. W. Landerer (2014), Seasonal variation in total water storage in California inferred from GPS observations of vertical land motion, Geophys. Res. Lett., 41, doi:10.1002/ 2014GL059570.

Argus, D. F., F. W. Landerer, D. N. Wiese, H. R. Martens, Y. Fu, J. S. Famiglietti, B. F. Thomas, T. G. Farr, A. W. Moore and M. M. Watkins (2017), Sustained Water Loss in California's Mountain Ranges During Severe Drought From 2012 to 2015 Inferred From GPS. J. Geophys. Res. Solid Earth, 122, 10,559-10,585. https://doi.org/10.1002/2017JB014424.

Austermann, J., Chen, C. Y., Lau, H. C., Maloof, A. C., & Latychev, K. (2020). Constraints

on mantle viscosity and Laurentide ice sheet evolution from pluvial paleolake shorelines in the western United States. Earth and Planetary Science Letters, 532, 116006.

Barbot, S., Moore, J. D., & Lambert, V. (2017). Displacement and stress associated with distributed anelastic deformation in a half-space. Bulletin of the Seismological Society of America, 107(2), 821– 855.

Barletta, V. R., Ferrari, C., Diolaiuti, G., Carnielli, T., Sabadini, R., & Smiraglia, C. (2006). Glacier shrinkage and modeled uplift of the Alps. Geophysical Research Letters, 33(14).

Beeler N., Lockner D., 2003. Why earthquakes correlate weakly with the solid earth tides: effects of periodic stress on the rate and probability of earthquake occurrence, J. geophys. Res., 108(B8), doi:10.1029/2001JB001518.

Ben-Zion, Y., and P. Leary (1986), Thermoelastic strain in a half- space covered by unconsolidated material, Bull. Seismol. Soc. Am., 76, 1447–1460.

Ben-Zion, Y., and A. Allam (2013), Seasonal thermoelastic strain and postseismic effects in Parkfield borehole dilatometers, Earth Planet. Sci. Lett., 379, 120– 126.

Berger, J. (1975), A note on thermoelastic strains and tilts, J. Geophys. Res., 80, 274–277.

Bettinelli, P., J.-P. Avouac, M. Flouzat, L. Bollinger, G. Ramillien, S. Rajaure, and S. Sapkota (2008). Seasonal variations of seismicity and geodetic strain in the Himalaya induced by surface hydrology. Earth and Planetary Science Letters, 266(3-4), 332–344. https://doi.org/10.1016/j.epsl.2007.11.021.

Bevis, M., D. Alsdorf, E. Kendrick, L. P. Fortes, B. Forsberg, R. Smalley Jr., and J. Becker (2005), Seasonal fluctuations in the mass of the Amazon River system and Earth's elastic response, Geophys. Res. Lett., 32, L16308, doi:10.1029/2005GL023491.

Bills, B. G., K. D. Adams, and S. G. Wesnousky (2007), Viscosity structure of the crust and upper mantle in western Nevada from isostatic rebound patterns of Lake Lahontan shorelines, J. Geophys. Res., 112(B6, B06405), doi:10.1029/2005JB003941.

Bills, B. G., D. R. Currey, and G. A. Marshall (1994), Viscosity estimates for the crust and upper mantle from patterns of lacustrine shoreline deformation in the Eastern Great Basin, J. Geophys. Res., 99, 22059-22086.

Biot, Maurice Anthony. "Thermoelasticity and irreversible thermodynamics." Journal of applied physics 27.3 (1956): 240-253.

Blewitt, G., D. Lavallée, P. Clarke, and K. Nurudinov (2001), A new global model of Earth deformation: Seasonal cycle detected, Science, 294, 2342–2345, doi:10.1126/science.1065328.

Blewitt, G., W.C. Hammond, and C. Kreemer, 2018, Harnessing the GPS data explosion for interdisciplinary science. Eos, 99, https://doi.org/10.1029/2018EO104623.

Bollinger, L., Perrier, F., Avouac, J. P., Sapkota, S., Gautam, U. T. D. R., & Tiwari, D. R. (2007). Seasonal modulation of seismicity in the Himalaya of Nepal. Geophysical Research Letters, 34(8).

Borsa, A. A., D. C. Agnew, and D. R. Cayan (2014), Ongoing drought-induced uplift in the western United States, Science, 345, doi:10.1126/science.1260279.

Brandes, C., H. Steffen, R. Steffen, and P. Wu (2015), Intraplate seismicity in northern Central Europe is induced by the last glaciation, Geology, 43, 611– 614, doi:10.1130/G36710.1.

Brothers, D. S., K. M. Luttrell, and J. D. Chaytor (2013), Sea-level–induced seismicity and submarine landslide occurrence, Geology, 41(9), 979-982, doi:10.1130/G34410.1.

Brothers, D., D. Kilb, K. Luttrell, N. Driscoll, and G. Kent (2011), Loading of the San Andreas fault by flood-induced rupture of faults beneath the Salton Sea, Nature Geoscience, 4(7), 486-492, doi:10.1038/ngeo1184.

Boussinesq, J., 1885. Application des Potentiels a l'Etude de l'Equilibre et du Mouvement des Solides lastiques, p. 508 Gauthier-Villars, Paris.

Bürgmann, R., & Dresen, G. (2008). Rheology of the lower crust and upper mantle: Evidence from rock mechanics, geodesy, and field observations. Annu. Rev. Earth Planet. Sci., 36, 531-567.

Byerlee, J. D. (1978), Friction of rocks, Pure Appl. Geophys., 116, doi:10.1007/BF00876528.

Calais, E., A. M. Freed, R. B. Van Arnsdale, and S. Stein (2010), Triggering of New Madrid seismicity by late-Pleistocene erosion, Nature, 466, doi:10.1038/nature09258.

Carlson, G., Shirzaei, M., Werth, S., Zhai, G., & Ojha, C. (2020). Seasonal and long-term groundwater unloading in the Central Valley modifies crustal stress. Journal of Geophysical Re-

search: Solid Earth, 125(1), e2019JB018490.

Caron, L., Ivins, E. R., Larour, E., Adhikari, S., Nilsson, J., & Blewitt, G. (2018). GIA model statistics for GRACE hydrology, cryosphere, and ocean science. Geophysical Research Letters, 45, 2203–2212. https://doi.org/10.1002/2017GL076644

Cathles, L. M. (1975). Viscosity of the Earth's Mantle (Vol. 1362). Princeton University Press.

Chanard, K., J. P. Avouac, G. Ramillien, and J. Genrich (2014), Modeling deformation induced by seasonal variations of continental water in the Himalaya region: Sensitivity to Earth elastic structure, J. Geophys. Res. Solid Earth, 119, 5097–5113, doi:10.1002/2013JB010451

Chanard, K., Fleitout, L., Calais, E., Rebischung, P., & Avouac, J.-P. (2018a). Toward a global horizontal and vertical elastic load deformation model derived from GRACE and GNSS station position time series. Journal of Geophysical Research: Solid Earth, 123, 3225–3237. https://doi.org/10.1002/2017JB015245

Chanard, K., Fleitout, L., Calais, E., Barbot, S., & Avouac, J.-P. (2018b). Constraints on transient viscoelastic rheology of the asthenosphere from seasonal deformation. Geophysical Research Letters, 45, 2328–2338, https://doi.org/10.1002/2017GL076451.

Chanard K., Nicolas A., Hatano T., Petrelis F., Latour S., Vinciguerra S., Schubnel A., 2019. Sensitivity of acoustic emission triggering to small pore pressure cycling perturbations during brittle creep, Geophys. Res. Lett., 46(13), 7414–7423..10.1029/2019GL082093

Chanard K, Métois M, Rebischung P, Avouac J-P (2020) A warning against over-interpretation of seasonal signals measured by the Global Navigation Satellite System. Nat Commun 11:1375. https://doi.org/10.1038/s41467-020-15100-7

Chaussard, E., S. Wdowinski, E. Cabral-Cano, and F. Amelung (2014), Land subsidence in central Mexico detected by ALOS InSAR time-series, Remote Sens. Environ., 140, 94– 106, doi:10.1016/j.rse.2013.08.038.

Chaussard, E., & Farr, T. G. (2019). A new method for isolating elastic from inelastic deformation in aquifer systems: Application to the San Joaquin Valley, CA. Geophysical Research Letters, 46(19), 10800-10809.

Chen, J., Cazenave, A., Dahle, C., Llovel, W., Panet, I., Pfeffer, J., & Moreira, L. (2022). Applications and challenges of GRACE and GRACE follow-on satellite gravimetry. Surveys in Geophysics, 1-41.

Chmiel, M., Godano, M., Piantini, M., Brigode, P., Gimbert, F., Bakker, M., ... & Chapuis, M. (2022). Brief communication: Seismological analysis of flood dynamics and hydrologically triggered earthquake swarms associated with Storm Alex. Natural Hazards and Earth System Sciences, 22(5), 1541-1558.

Christiansen, L. B., S. Hurwitz, M. O. Saar, S. E. Ingebritsen, and P. A. Hsieh (2005), Seasonal seismicity at western United States volcanic centers, Earth Planet. Sci. Lett., 240, 307–321

Christiansen, L. B., S. Hurwitz, and S. E. Ingebritsen (2007), Annual modulation of seismicity along the San Andreas Fault near Parkfield, CA, Geophys. Res. Lett., 34(L04306), doi:10.1029/2006GL028634.

Cocco, M., and J. R. Rice (2002), Pore pressure and poroelasticity effects in Coulomb stress analysis of earthquake interactions, J. Geophys. Res., 107(B2), ESE 2-1-ESE 2-17, doi:10.1029/2000JB000138.

Cochran E.S., Vidale J.E., Tanaka S., 2004. Earth tides can trigger shallow thrust fault earthquakes, Science, 306(5699), 1164–1166..10.1126/science.1103961

Compton, K., R. A. Bennett, and S. Hreinsdóttir (2015), Climate-driven vertical acceleration of Icelandic crust measured by continuous GPS geodesy, Geophys. Res. Lett.,42, 743–750, doi:10.1002/2014GL062446.

Craig, T. J., E. Calais, L. Fleitout, L. Bollinger, and O. Scotti (2016), Evidence for the release of long-term tectonic strain stored in continental interiors through intraplate earthquakes, Geophys. Res. Lett., 43, 6826–6836, doi:10.1002/2016GL069359.

Craig, T. J., K. Chanard, and E. Calais (2017). Hydrologically-driven crustal stresses and seismicity in the New Madrid Seismic Zone. Nature Communications, 8(1), 2143. https://doi.org/10.1038/s41467-017-01696-w.

Dai, A. (2016). Historical and future changes in streamflow and continental runoff: A review. Terrestrial Water Cycle and Climate Change: Natural and Human-Induced Impacts, 17-37.

D'Agostino, N., Silverii, F., Amoroso, O., Convertito, V., Fiorillo, F., Ventafridda, G., and Zollo, A.: Crustal Deformation and Seismicity Modulated by Groundwater Recharge of Karst Aquifers, Geophys. Res. Lett., 45, 12253–12262, https://doi.org/10.1029/2018GL079794, 2018.

Darwin G.H.; 1882: XLVI. On variation of the vertical due to elasticity of the Earth's surface. Philosophical Magazine Series 5, 14, 409-427, doi: 10.1080/14786448208628439.

Davis, J. L., P. Elósegui, J. X. Mitrovica, and M. E. Tamisiea (2004), Climate-driven deformation of the solid Earth from GRACE and GPS, Geophys. Res. Lett., 31, L24605, doi:10.1029/2004GL021435.

Dietrich, R., Ivins, E. R., Casassa, G., Lange, H., Wendt, J., & Fritsche, M. (2010). Rapid crustal uplift in Patagonia due to enhanced ice loss. Earth and Planetary Science Letters, 289(1-2), 22-29.

Dong, D., Fang, P., Bock, Y., Cheng, M. K., & Miyazaki, S. I. (2002). Anatomy of apparent seasonal variations from GPS-derived site position time series. Journal of Geophysical Research: Solid Earth, 107(B4), ETG-9.

Dublanchet, P. (2022). Seismicity modulation in a 3-D rate-and-state interacting fault population model. Geophysical Journal International, 229(3), 1804-1823.

Dutilleul, P., Johnson, C. W., Bürgmann, R., Wan, Y., & Shen, Z. K. (2015). Multifrequential periodogram analysis of earthquake occurrence: An alternative approach to the Schuster spectrum, with two examples in central California. Journal of Geophysical Research: Solid Earth, 120(12), 8494-8515.

Drake, N. F. (1912). Destructive earthquakes in China. Bulletin of the Seismological Society of America, 2(1), 40-91.

Dziewonski, A., and D. L. Anderson (1981), Preliminary reference Earth model, Phys. Earth Planet. Inter., 25, 297–356.

Enzminger, T. L., E. E. Small, and A. A. Borsa (2018). Accuracy of snow water equivalent estimated from GPS vertical displacements: A synthetic loading case study for western U.S. mountains. Water Resources Research,54, 581–599. https://doi.org/10.1002/2017WR021521.

Fallou, L., M. Marti, I. Dallo, and M. Corradini (2022), How to Fight Earthquake Misinformation: A Communication Guide, Seismological Research Letters, 93(5), 2418-2422, doi:10.1785/0220220086.

Fang, M., Dong, D. N., & Hager, B. H. (2014). Displacements due to surface temperature variation on a uniform elastic sphere with its centre of mass stationary. Geophysical Journal International, 196(1), 194– 203. https://doi.org/10.1093/gji/ggt335

Farrell, W. E. (1972), Deformation of the Earth by surface loads, Rev. Geophys. Space Phys., 10, 761–797, doi:10.1029/RG010i003p00761.

Faunt, C. C., Sneed, M., Traum, J., & Brandt, J. T. (2016). Water availability and land subsidence in the Central Valley, California, USA. Hydrogeology Journal, 24(3), 675-684.

Frederikse, T., Landerer, F., Caron, L., Adhikari, S., Parkes, D., Humphrey, V. W., ... & Wu, Y. H. (2020). The causes of sea-level rise since 1900. Nature, 584(7821), 393-397.

Freed, A. M., and R. Bürgmann (2004), Evidence of power law flow in the Mojave desert mantle, Nature, 430(doi:10.1038/nature02784), 548-551.

Friedrich, A.M., Wernicke, B.P., Niemi, N.A., Bennett, R.A., Davis, J.L., 2003. Comparison of geodetic and geologic data from the Wasatch region, Utah, and implications for the spectral character of Earth deformation at periods of 10 to 10 million years. J. Geophys. Res. 108 (B4), 2199

Fu, Y., and J. T. Freymueller (2012a), Seasonal and long-term vertical deformation in the Nepal Himalaya constrained by GPS and GRACE measurements, J. Geophys. Res., 117, B03407, doi:10.1029/2011JB008925.

Fu, Y., J. T. Freymueller, and T. Jensen (2012b), Seasonal hydrological loading in southern Alaska observed by GPS and GRACE, Geophys. Res. Lett., 39, L15310, doi:10.1029/2012GL052453.

Fu, Y., D. F. Argus and F. W. Landerer (2015), GPS As an Independent Measurement to Estimate Terrestrial Water Storage Variations in Washington and Oregon, J. Geophys. Res. Solid Earth, 120, 552-566, doi:10.1002/2014JB011415. Galloway, D. L., Jones, D. R., & Ingebritsen, S. E. (Eds.). (1999). Land subsidence in the United States (Vol. 1182). US Geological Survey.

Gao, S. S., Silver, P. G., Linde, A. T., & Sacks, I. S. (2000). Annual modulation of triggered seismicity following the 1992 Landers earthquake in California. Nature, 406(6795), 500–504,

doi.org/10.1038/35020045

Gauer, L. M., Chanard, K., & Fleitout, L. (2023). Data-driven gap filling and spatio-temporal filtering of the GRACE and GRACE-FO records. Journal of Geophysical Research: Solid Earth, e2022JB025561.

Gilbert, G. K. (1890), Lake Bonneville, USGS Monograph, 1, doi:10.3133/m1.

Gonzalez, P., Tiampo, K., Palano, M., Cannav., F., Fernandez, J., 2012. The 2011 Lorca earthquake slip distribution controlled by groundwater crustal unloading. Nat. Geosci. 5, 821–825.

Gradmann, S., Olesen, O., Keiding, M. and Maystrenko, Y. (2018). The regional 3D stress field of Nordland, northern Norway – insights from numerical modelling. In O. Olesen et al., eds., Neotectonics in Nordland – Implications for petroleum exploration (NEONOR2). NGU Report 2018.010, 215–240.

Grapenthin, R., F. Sigmundsson, H. Geirsson, T. Árnadóttir, and V. Pinel (2006), Icelandic rhythmics: Annual modulation of land elevation and plate spreading by snow load, Geophys. Res. Lett., 33, L24305, doi:10.1029/2006GL028081.

Green, Timothy R., Makoto Taniguchi, Henk Kooi, Jason J. Gurdak, Diana M. Allen, Kevin M. Hiscock, Holger Treidel, and Alice Aureli (2011), "Beneath the surface of global change: Impacts of climate change on groundwater." Journal of Hydrology 405, no. 3-4: 532-560.

Gregersen, S., LIndholm, C., Korja, A., Lund, B., Uski, M., Oinonen, K., ... & Kieding, M. (2021). Seismicity and sources of stress in Fennoscandia. Glacially-Triggered Faulting.

Grollimund, B., and M. D. Zoback (2001), Did deglaciation trigger New Madrid seismicity?, Geology, 29, 175-178.

Gudmundsson, L., Leonard, M., Do, H. X., Westra, S., & Seneviratne, S. I. (2019). Observed trends in global indicators of mean and extreme streamflow. Geophysical Research Letters, 46(2), 756-766.

Hainzl, S., Kraft, T., Wassermann, J., Igel, H., Schmedes, E., 2006. Evidence for rainfall triggered earthquake activity. Geophys. Res. Lett. 33, L19303.

Hansen, L. N., Zimmerman, M. E., & Kohlstedt, D. L. (2011). Grain boundary sliding in San Carlos olivine: Flow law parameters and crystallographic-preferred orientation. Journal of Geophysical Research: Solid Earth, 116(B8). Hampel, A., R. Hetzel, G. Maniatis, and T. Karow (2009), Three-dimensional numerical modeling of slip rate variations on normal and thrust fault arrays during ice cap growth and melting, J. Geophys. Res., 114, B08406, doi:10.1029/2008JB006113.

Hampel, A., Hetzel, R., Maniatis, G., 2010. Response of faults to climate-driven changes in ice and water volumes on Earth's surface. Philos. Trans. R. Soc., Math. Phys. Eng. Sci. 368 (1919), 2501–2517.

Haskell, N. A. (1935), The motion of a fluid under a surface load, Physics, 6, 256.

Heaton T.H., 1982. Tidal triggering of earthquakes, Bull. seism. Soc. Am., 72(6A), 2181–2200..10.1785/BSSA07206A2181

Heimisson E.R., Segall P., 2018. Constitutive law for earthquake production based on rate-and-state friction: Dieterich 1994 revisited, J. geophys. Res., 123(5)

Heimisson E.R., Avouac J.-P., 2020. Analytical prediction of seismicity rate due to tides and other oscillating stresses, Geophys. Res. Lett., 47(23), e2020GL090827, doi:10.1029/2020GL090827.

Heki, K. (2003). Snow load and seasonal variation of earthquake occurrence in Japan. Earth and Planetary Science Letters, 207(1-4), 159–164. https://doi.org/10.1016/S0012-821X(02)01148-2.

Heki, K. (2004), Dense GPS array as a new sensor of seasonal changes of surface loads, in The State of the Planet: Frontiers and Challenges in Geophysics, Geophys. Monogr. Ser., vol. 150, edited by R. S. J. Sparks and C. J.

Hawkesworth, pp. 177–196, AGU, Washington, D. C., doi:10.1029/150GM15.

Heki, K., & Arief, S. (2022). Crustal response to heavy rains in Southwest Japan 2017-2020. Earth and Planetary Science Letters, 578, 117325.

Hersbach, H., Bell, B., Berrisford, P., Hirahara, S., Horányi, A., Muñoz-Sabater, J., ... & Thépaut, J. N. (2020). The ERA5 global reanalysis. Quarterly Journal of the Royal Meteorological Society, 146(730), 1999-2049.

Hetzel, R., Hampel, A. (2005). Slip rate variations on normal faults during glacial–interglacial

changes in surface loads. Nature 435, 81–84.

Hill, R. G., M. Weingarten, T. K. Rockwell, and Y. Fialko (2023), Major southern San Andreas earthquakes modulated by lake-filling events, Nature, 618(7966), 761-766, doi:10.1038/s41586-023-06058-9.

Hirth, G., & Kohlstedt, D. (2003). Rheology of the upper mantle and the mantle wedge: A view from the experimentalists. Geophysical monograph-american geophysical union, 138, 83-106.

Hsu, Y. J., Chang, Y. S., Liu, C. C., Lee, H. M., Linde, A. T., Sacks, S. I., et al. (2015). Revisiting borehole strain, typhoons, and slow earthquakes using quantitative estimates of precipitation-induced strain changes. Journal of Geophysical Research: Solid Earth, 120, 4556– 4571. https://doi.org/10.1002/2014JB011807.

Hsu, Y. J., Kao, H., Bürgmann, R., Lee, Y. T., Huang, H. H., Hsu, Y. F., et al. (2021). Synchronized and asynchronous modulation of seismicity by hydrological loading: A case study in Taiwan. Science Advances, 7(16), eabf7282. https://doi.org/10.1126/sciadv.abf7282

Hu, X., & Bürgmann, R. (2020). Aquifer deformation and active faulting in Salt Lake Valley, Utah, USA. Earth and Planetary Science Letters, 547, 116471. doi: 10.1016/J.EPSL.2020.116471.

Hu, X., Xue, L., Bürgmann, R., & Fu, Y. (2021). Stress perturbations from hydrological and industrial loads and seismicity in the Salt Lake City region. Journal of Geophysical Research: Solid Earth, 126, e2021JB022362. https://doi. org/10.1029/2021JB022362

Hu, Y., & Freymueller, J. T. (2019). Geodetic observations of time-variable glacial isostatic adjustment in Southeast Alaska and its implications for Earth rheology. Journal of Geophysical Research: Solid Earth, 124(9), 9870-9889.

Hugonnet, R., McNabb, R., Berthier, E., Menounos, B., Nuth, C., Girod, L., ... & Kääb, A. (2021). Accelerated global glacier mass loss in the early twenty-first century. Nature, 592(7856), 726-731.

Husen, S., Bachmann, C., & Giardini, D. (2007). Locally triggered seismicity in the central Swiss Alps following the large rainfall event of August 2005. Geophysical Journal International, 171(3), 1126-1134.

The IMBIE team. Mass balance of the Antarctic Ice Sheet from 1992 to 2017. Nature 558, 219–222 (2018). https://doi.org/10.1038/s41586-018-0179-y

The IMBIE Team. Mass balance of the Greenland Ice Sheet from 1992 to 2018. Nature 579, 233–239 (2020). https://doi.org/10.1038/s41586-019-1855-2

IPCC, 2021: Climate Change 2021: The Physical Science Basis. Contribution of Working Group I to the Sixth Assessment Report of the Intergovernmental Panel on Climate Change [Masson-Delmotte, V., P. Zhai, A. Pirani, S.L. Connors, C. Péan, S. Berger, N. Caud, Y. Chen, L. Goldfarb, M.I. Gomis, M. Huang, K. Leitzell, E. Lonnoy, J.B.R. Matthews, T.K. Maycock, T. Waterfield, O. Yelekçi, R. Yu, and B. Zhou (eds.)]. Cambridge University Press, Cambridge, United Kingdom and New York, NY, USA, In press, doi:10.1017/9781009157896.

IPCC, 2022: Climate Change 2022: Impacts, Adaptation, and Vulnerability. Contribution of Working Group II to the Sixth Assessment Report of the Intergovernmental Panel on Climate Change [H.-O. Pörtner, D.C. Roberts, M. Tignor, E.S. Poloczanska, K. Mintenbeck, A. Alegría, M. Craig, S. Langsdorf, S. Löschke, V. Möller, A. Okem, B. Rama (eds.)]. Cambridge University Press. In Press.

Ivins, E. R., T. S. James, J. Wahr, E. J. O. Schrama, F. W. Landerer, and K. M. Simon (2013), Antarctic contribution to sea level rise observed by GRACE with improved GIA correction,J. Geophys. Res. Solid Earth,118,3126–3141, doi:10.1002/jgrb.50208.

Ivins, E. R., James, T. S., & Klemann, V. (2003). Glacial isostatic stress shadowing by the Antarctic ice sheet. Journal of Geophysical Research: Solid Earth, 108(B12).

Johnston, A. C. (1987). Suppression of earthquakes by large continental ice sheets. Nature, 330(6147), 467-469.

Johnson, C. W., Y. Fu, R. Bürgmann (2017a), Seasonal water storage, stress modulation, and California seismicity, Science, 356, 1161–1164, doi: 10.1126/science.aak9547.

Johnson, C. W., Y. Fu, R. Bürgmann (2017b), Stress models of the annual hydrospheric, atmospheric, thermal, and tidal loading cycles on California faults: Perturbation of background stress and changes in seismicity J. Geophys. Res., 122, 10,605–10,625. https://doi.org/10.1002/2017JB014778.

Johnson, C. W., Y. Fu and R. Bürgmann (2020), Hydrospheric modulation of stress and seismicity on shallow faults in southern Alaska. Earth Planet. Sci. Lett., 530, 115904, doi:10.1016/j.epsl.2019.115904.

Kääb, A., Leinss, S., Gilbert, A., Bühler, Y., Gascoin, S., Evans, S. G., ... & Yao, T. (2018). Massive collapse of two glaciers in western Tibet in 2016 after surge-like instability. Nature Geoscience, 11(2), 114-120.

Kierulf, Halfdan Pascal, et al. (2021), A GNSS velocity field for geophysical applications in Fennoscandia. Journal of Geodynamics 146: 101845.

Kim, J., Holt, W. E., Bahadori, A., & Shen, W. (2021a). Repeating nontectonic seasonal stress changes and a possible triggering mechanism of the 2019 Ridgecrest earthquake sequence in California. Journal of Geophysical Research: Solid Earth, 126, e2021JB022188. https://doi.org/10.1029/2021JB022188.

Kim, J., Bahadori, A., & Holt, W. E. (2021b). Crustal strain patterns associated with normal, drought, and heavy precipitation years in California. Journal of Geophysical Research: Solid Earth, 126, e2020JB019560. https://doi.org/10.1029/2020JB019560

Klemann, V., and Wolf, D., 1998, Modelling of stresses in the Fennoscandian lithosphere induced by Pleistocene glaciations: Tectonophysics, v. 294, p. 291–303, doi:10.1016/S0040-1951(98)00107-3.

Knowles, L. A., R. A. Bennett, and C. Harig (2020). Vertical displacements of the Amazon Basin from GRACE and GPS. Journal of Geophysical Research: Solid Earth, 125(2). https://doi.org/10.1029/2019JB018105.

Kraft, J. Wassermann, E. Schmedes, H. Igel, Meteorological triggering of earthquake swarms at Mt. Hochstaufen, SE-Germany, Tectonophysics, Volume 424, Issues 3–4, 2006, Pages 245-258, ISSN 0040-1951, https://doi.org/10.1016/j.tecto.2006.03.044.

Kraner, M. L., Holt, W. E., & Borsa, A. A. (2018). Seasonal nontectonic loading inferred from cGPS as a potential trigger for the M6.0 South Napa earthquake. Journal of Geophysical Research: Solid Earth, 123(6), 5300– 5322. https://doi.org/10.1029/2017JB015420

Kreemer, C., & Zaliapin, I. (2018). Spatio-temporal correlation between seasonal variations in seismicity and horizontal dilatational strain in California. Geophysical Research Letters, 45, 9559– 9568. https://doi.org/10.1029/2018GL079536

Kundu, B., N. K. Vissa, and V. K. Gahalaut (2015), Influence of anthropogenic groundwater unloading in Indo-Gangetic plains on the 25 April 2015 Mw 7.8 Gorkha, Nepal earthquake, Geophys. Res. Lett., 42, doi:10.1002/2015GL066616.

Kundu, B., N. K. Vissa, K. Gahalaut, V. K. Gahalaut, D. Panda, and K. Malik (2019), Influence of anthropogenic groundwater pumping on the 2017 November 12 M7.3 Iran–Iraq border earthquake, Geophys. J. Int., 218(2), 833-839, doi:10.1093/gji/ggz195.

Lambeck, K., and J. Chappell (2001), Sea level change through the last glacial cycle, Science, 292(5517), 679–686.

Lambeck, K., and A. Purcell (2003), Glacial rebound and crustal stress in Finland, Tech. Rep., Oliluoto, Finland.

Landerer, F. W., Flechtner, F. M., Save, H., Webb, F. H., Bandikova, T., Bertiger, W. I., ... & Yuan, D. N. (2020). Extending the global mass change data record: GRACE Follow-On instrument and science data performance. Geophysical Research Letters, 47(12), e2020GL088306.

Larochelle, S., Chanard, K., Fleitout, L., Fortin, J., Gualandi, A., Longuevergne, L., ... & Avouac, J. P. (2022). Understanding the geodetic signature of large aquifer systems: Example of the Ozark Plateaus in Central United States. Journal of Geophysical Research: Solid Earth, 127(3), e2021JB023097.

Larsen, C. F., Motyka, R. J., Freymueller, J. T., Echelmeyer, K. A., & Ivins, E. R. (2005). Rapid viscoelastic uplift in southeast Alaska caused by post-Little Ice Age glacial retreat. Earth and Planetary Science Letters, 237(3-4), 548– 560. https://doi.org/10.1016/j.epsl.2005.06.032

Lau, H. C., Mitrovica, J. X., Austermann, J., Crawford, O., Al-Attar, D., & Latychev, K. (2016). Inferences of mantle viscosity based on ice age data sets: Radial structure. Journal of Geophysical Research: Solid Earth, 121(10), 6991-7012.

Lau, H. C., & Holtzman, B. K. (2019). "Measures of dissipation in viscoelastic media" extended: Toward continuous characterization across very broad geophysical time scales. Geophysical Research Letters, 46(16), 9544-9553.

Lau, H. C., Austermann, J., Holtzman, B. K., Havlin, C., Lloyd, A. J., Book, C., & Hopper, E. (2021). Frequency Dependent Mantle Viscoelasticity via the Complex Viscosity: Cases From Antarctica. Journal of Geophysical Research: Solid Earth, 126(11), e2021JB022622.

Li, W., van Dam, T., Li, Z., & Shen, Y. (2016). Annual variation detected by GPS, GRACE and loading models. Studia Geophysica et Geodaetica, 60, 608-621.

Liu, C., Linde, A. T., & Sacks, I. S. (2009). Slow earthquakes triggered by typhoons. Nature, 459(7248), 833-836.

Longman, I. (1962), A Green's function for determining the deformation of the Earth under surface mass loads: 1. Theory, J. Geophys. Res., 67(2), 845–850.

Longman, I. (1963), A Green's function for determining the deformation of the Earth under surface mass loads: 2. Computations and numerical results, J. Geophys. Res., 68(2), 485–49.

Lough, A. C., Wiens, D. A., & Nyblade, A. (2018). Reactivation of ancient Antarctic rift zones by intraplate seismicity. Nature Geoscience, 11(7), 515-519.

Lowry A.R., 2006. Resonant slow fault slip in subduction zones forced by climatic load stress, Nature, 442(7104), 802–805..10.1038/nature05055

Lund, B., P. Schimdt, and C. Hieronymus (2009), Stress Evolution and Fault Stability During the Weichselian Glacial Cycle, Swedish Nucl. Fuel and Waste Manage. Co (SKB), Stockholm, Sweden.

Lundgren, P., Liu, Z., & Ali, S. T. (2022). San Andreas Fault Stress Change Due To Groundwater Withdrawal in California's Central Valley, 1860-2010. Geophysical Research Letters, 49(3), e2021GL095975.

Luttrell, K., and Sandwell, D., 2010, Ocean loading effects on stress at near shore plate boundary fault systems: Journal of Geophysical Research, v. 115, B08411, doi:10.1029/2009JB006541.

Martens, H. R., Rivera, L., & Simons, M. (2019). LoadDef: A Python-based toolkit to model elastic deformation caused by surface mass loading on spherically symmetric bodies. Earth and Space Science, 6(2), 311– 323. https://doi.org/10.1029/2018EA000462

Martin-Español, A., Bamber, J. L., & Zammit-Mangion, A. (2017). Constraining the mass balance of East Antarctica. Geophysical Research Letters, 44, 4168– 4175. https://doi.org/10.1002/2017GL072937.

Melini D., Gegout P., Spada G, King M. (2014) REAR - a regional ElAstic Rebound calculator. User manual for version 1.0, available on–line at: http://hpc.rm.ingv.it/rear.

Meng, X., Yang, H., & Peng, Z. (2018). Foreshocks, b valuemap, and aftershock triggering for the 2011 Mw 5.7 Virginia earthquake. Journal of Geophysical Research: Solid Earth, 123, 5082–5098. https://doi.org/10.1029/2017JB015136

Michel, A., & Boy, J. P. (2022). Viscoelastic Love numbers and long-period geophysical effects. Geophysical Journal International, 228(2), 1191-1212.

Miller, S. A. (2008), Note on rain-triggered earthquakes and their dependence on karst geology, Geophys. J. Int., 173(1), 334-338, doi:10.1111/j.1365-246X.2008.03735.x.

Milliner, C., K. Materna, R. Bürgmann, Y. Fu, A. W. Moore, D. Bekaert, S. Adhikari and D. F. Argus (2018), Tracking the Weight of Hurricane Harvey's Stormwater Using GPS data. Sci. Adv., 4, eaau2477, doi:10.1126/sciadv.aau2477.

Milne, G. A., Davis, J. L., Mitrovica, J. X., Scherneck, H. G., Johansson, J. M., Vermeer, M., & Koivula, H. (2001). Space-geodetic constraints on glacial isostatic adjustment in Fennoscandia. Science, 291(5512), 2381-2385. Missiakoulis, S. (2008). Aristotle and earthquake data: A historical note. International Statistical Review, 76(1), 130-133.

Mitrovica, J. X., & Forte, A. M. (2004). A new inference of mantle viscosity based upon joint inversion of convection and glacial isostatic adjustment data. Earth and Planetary Science Letters, 225(1-2), 177-189. Mogi, K. (1958), Relations between the eruptions of various volcanoes and the deformations of the ground surfaces around them, Bull. Earthquake Res. Inst. Univ. Tokyo, 36, 99-134.

Montgomery-Brown, E. K., Shelly, D. R., & Hsieh, P. A. (2019). Snowmelt-triggered earthquake swarms at the margin of Long Valley Caldera, California. Geophysical Research Letters, 46, 3698– 3705. https://doi.org/10.1029/2019GL082254

Mouginot, J., Rignot, E., Bjørk, A. A., Van den Broeke, M., Millan, R., Morlighem, M., ... & Wood, M. (2019). Forty-six years of Greenland Ice Sheet mass balance from 1972 to 2018.

Proceedings of the national academy of sciences, 116(19), 9239-9244.

Munier, R., Adams, J., Brandes, C., Brooks, G., Dehls, J., Gibbons, S. J., ... & Tassis, G. (2020). International Database of Glacially Induced Faults. PANGAEA.

Nield, G. A., Barletta, V. R., Bordoni, A., King, M. A., Whitehouse, P. L., Clarke, P. J., ... & Berthier, E. (2014). Rapid bedrock uplift in the Antarctic Peninsula explained by viscoelastic response to recent ice unloading. Earth and Planetary Science Letters, 397, 32-41.

Noël, C., Pimienta, L., & Violay, M. (2019). Time-dependent deformations of sandstone during pore fluid pressure oscillations: Implications for natural and induced seismicity. Journal of Geophysical Research: Solid Earth, 124(1), 801-821.

Olivieri, M., & Spada, G. (2015). Ice melting and earthquake suppression in Greenland. Polar science, 9(1), 94-106.

Ojha, C., M. Shirzaei, S. Werth, D. F. Argus, and T. G. Farr (2018), Sustained groundwater loss in California's Central Valley exacerbated by intense drought periods. Water Resources Research, 54. https://doi.org/10.1029/2017WR022250.

Ojha, C., Werth, S., & Shirzaei, M. (2019). Groundwater loss and aquifer system compaction in San Joaquin Valley during 2012–2015 drought. Journal of Geophysical Research: Solid Earth, 124(3), 3127-3143.

Otto, F. E. L. (2017), Attribution of Weather and Climate Events, Annual Review of Environment and Resources, 42(1), 627-646, doi:10.1146/annurev-environ-102016-060847.

Ouellette, K. J., C. de Linage, and J. S. Famiglietti (2013), Estimating snow water equivalent from GPS vertical site-position observations in the western United States, Water Resour. Res., 49, 2508–2518, doi:10.1002/wrcr.20173.

Pagli C, Sigmundsson F (2008) Will present day glacier retreat increase volcanic activity? Stress induced by recent glacier retreat and its effect on magmatism at the Vatnajokull ice cap. Iceland. Iceland 35:L09304. doi:10.1029/2008GL033510

Peltier, W. R., & Andrews, J. T. (1976). Glacial-isostatic adjustment—I. The forward problem. Geophysical Journal International, 46(3), 605-646.

Perfettini H., Schmittbuhl J., Rice J.R., Cocco M., 2001. Frictional response induced by time-dependent fluctuations of the normal loading, J. geophys. Res., 106(B7), 13 455–13 472..10.1029/2000JB900366

Perfettini H., Schmittbuhl J., Cochard A., 2003. Shear and normal load perturbations on a two-dimensional continuous fault: 2. Dynamic triggering, J. geophys. Res., 108(B9), doi:10.1029/2002JB001805.

Pétrélis, F., Chanard, K., Schubnel, A., & Hatano, T. (2021). Earthquake sensitivity to tides and seasons: Theoretical studies. Journal of Statistical Mechanics: Theory and Experiment, 2021(2), 023404.

Pisarska-Jamroży, M., Belzyt, S., Börner, A. et al. (2018). Evidence from seismites for glacio-isostatically induced crustal faulting in front of an advancing land-ice mass (Rügen Island, SW Baltic Sea). Tectonophysics, 745, 338–348, doi.org/10.1016/j.tecto.2018.08.004.

Pollitz, F. F. (1996). Coseismic deformation from earthquake faulting on a spherical Earth. Geophysical Journal International, 125(1), 1–14. https://doi.org/10.1111/j.1365- 246X.1996.tb06530.x.

Pollitz, F., L. Kellogg, and R. Bürgmann (2001), Sinking mafic body in a reactivated lower crust: A mechanism for stress concentration in the New Madrid Seismic Zone, Bull. Seism. Soc. Am., 91, 1882-1897.

Pollitz, F. F. (2003). Transient rheology of the uppermost mantle beneath the Mojave Desert, California. Earth and Planetary Science Letters, 215(1-2), 89-104.

Pollitz, F. F., A. G. Wech, H. Kao, and R. Bürgmann (2013), Annual modulation of non-volcanic tremor in northern Cascadia, J .Geophys. Res., 118, doi:10.1002/jgrb.50181.

Prawirodirdjo, L., Y. Ben-Zion, and Y. Bock (2006), Observation and modeling of thermoelastic strain in Southern California Integrated GPS Network daily position time series, J. Geophys. Res., 111, B02408, doi:10.1029/2005JB003716.

Qin, L., Ben-Zion, Y., Qiu, H., Share, P. E., Ross, Z. E., & Vernon, F. L. (2018). Internal structure of the San Jacinto fault zone in the trifurcation area southeast of Anza, California, from data of dense seismic arrays. Geophysical Journal International, 213(1), 98-114.

Reasenberg, P. (1985). Second-order moment of central California seismicity, 1969–1982. Journal of Geophysical Research: Solid Earth, 90(B7), 5479-5495.

Rice, J. R., and M. P. Cleary (1976), Some basic stress diffusion solutions for fluid-saturated elastic porous media with compressible constituents, Rev. Geophys. Space Phys., 14, 227–241.

Rigo, A., Béthoux, N., Masson, F., & Ritz, J. F. (2008). Seismicity rate and wave-velocity variations as consequences of rainfall: the case of the catastrophic storm of September 2002 in the Nîmes Fault region (Gard, France). Geophysical Journal International, 173(2), 473-482.

Rodell, M., Houser, P. R., Jambor, U. E. A., Gottschalck, J., Mitchell, K., Meng, C. J., ... & Toll, D. (2004). The global land data assimilation system. Bulletin of the American Meteorological society, 85(3), 381-394.

Rollins, C., Freymueller, J. T., & Sauber, J. M. (2021). Stress Promotion of the 1958 Mw∼ 7.8 Fairweather Fault Earthquake and Others in Southeast Alaska by Glacial Isostatic Adjustment and Inter-earthquake Stress Transfer. Journal of Geophysical Research: Solid Earth, 126(1), e2020JB020411.

Saar, M. O., and Manga, M. (2003). Seismicity Induced by Seasonal GroundwaterRecharge at Mt. Hood, Oregon. Earth Planet. Sci. Lett. 214, 605–618.doi:10.1016/S0012-821X(03)00418-7

Sauber, J., Plafker, G., Molnia, B. F., & Bryant, M. A. (2000). Crustal deformation associated with glacial fluctuations in the eastern Chugach Mountains, Alaska. Journal of Geophysical Research: Solid Earth, 105(B4), 8055-807

Sauber, J. M., & Molnia, B. F. (2004). Glacier ice mass fluctuations and fault instability in tectonically active Southern Alaska. Global and Planetary Change, 42(1-4), 279-293.

Sauber, J., & Ruppert, N. A. (2008). Rapid ice mass loss: Does it have an influence on earthquake occurrence in southern Alaska. Active Tectonics and Seismic Potential of Alaska, Geophysical Monograph Series, 369-384.

Sauber, J., C. Rollins, J. T. Freymueller, and N. A. Ruppert (2021), Glacially Induced Faulting in Alaska, in Glacially-Triggered Faulting, edited by H. Steffen, O. Olesen and R. Sutinen, pp. 353-365, Cambridge University Press, Cambridge, doi:DOI: 10.1017/9781108779906.026.

Sayles, R. W. (1913). Earthquakes and rainfall. Bulletin of the Seismological Society of America, 3(2), 5

Scholz C.H., Tan Y.J., Albino F., (2019). The mechanism of tidal triggering of earthquakes at mid-ocean ridges, Nat. Commun., 10(1), 1–7..10.1038/s41467-019-10605-2

Schulz, W. H., McKenna, J. P., Kibler, J. D., & Biavati, G. (2009). Relations between hydrology and velocity of a continuously moving landslide—evidence of pore-pressure feedback regulating landslide motion?. Landslides, 6(3), 181-190.

Schuster, A. (1897). On lunar and solar periodicities of earthquakes. Proceedings of the Royal Society of London, 61(369-377), 455-465.

Schuster, A. (1898). On the investigation of hidden periodicities with application to a supposed 26 day period of meteorological phenomena. Terrestrial Magnetism, 3(1), 13-41.

Sella, Giovanni F., et al. "Observation of glacial isostatic adjustment in "stable" North America with GPS." Geophysical Research Letters 34.2 (2007).

Senapati, B., B. Kundu, and S. Jin (2022), Seismicity modulation by external stress perturbations in plate boundary vs. stable plate interior, Geoscience Frontiers, 13(3), 101352, doi:https://doi.org/10.1016/j.gsf.2022.101352. Shepherd, A., Ivins, E. R., Barletta, V. R., Bentley, M. J., Bettadpur, S., Briggs, K. H., ... & Zwally, H. J. (2012). A reconciled estimate of ice-sheet mass balance. Science, 338(6111), 1183-1189.

Shirzaei, M., Freymueller, J., Törnqvist, T. E., Galloway, D. L., Dura, T., & Minderhoud, P. S. (2021). Measuring, modelling and projecting coastal land subsidence. Nature Reviews Earth & Environment, 2(1), 40-58.

Sigmundsson, F., Pinel, V., Lund, B., Albino, F., Pagli, C., Geirsson, H., & Sturkell, E. (2010). Climate effects on volcanism: influence on magmatic systems of loading and unloading from ice mass variations, with examples from Iceland. Philosophical Transactions of the Royal Society A: Mathematical, Physical and Engineering Sciences, 368(1919), 2519-2534.

Silverii, F., Montgomery-Brown, E. K., Borsa, A. A., & Barbour, A. J. (2020). Hydrologically induced deformation in Long Valley Caldera and adjacent Sierra Nevada. Journal of Geophysical Research: Solid Earth, 125, e2020JB019495. https://doi.org/10.1029/2020JB019495

Smith, R. G., Knight, R., Chen, J., Reeves, J. A., Zebker, H. A., Farr, T., & Liu, Z. (2017).

Estimating the permanent loss of groundwater storage in the southern San Joaquin Valley, California. Water Resources Research, 53(3), 2133-2148.

Smith, R. G., Hashemi, H., Chen, J., & Knight, R. (2021). Apportioning deformation among depth intervals in an aquifer system using InSAR and head data. Hydrogeology Journal, 29(7), 2475-2486.

Steer, P., M. Simoes, R. Cattin, and J. B. H. Shyu (2014), Erosion influences the seismicity of active thrust faults, Nat. Commun., 5, doi:10.1038/ncomms6564.

Steer, P., Jeandet, L., Cubas, N., Marc, O., Meunier, P., Simoes, M., et al. (2020). Earthquake statistics changed by typhoon-driven erosion. Scientific Reports, 10(1), 1–11. https://doi.org/10.1038/s41598-020-67865-y

Steffen, R., Wu, P., Steffen, H., Eaton, D.W. (2014): The effect of earth rheology and ice-sheet size on fault-slip and magnitude of postglacial earthquakes. Earth and Planetary Science Letters, 388, 71-80, doi:10.1016/j.epsl.2013.11.058.

Steffen, H., Olesen, O., & Sutinen, R. (2021). Glacially Triggered Faulting: A Historical Overview and Recent Developments. In H. Steffen, O. Olesen, & R. Sutinen (Eds.), Glacially-Triggered Faulting (pp. 3-19). Cambridge: Cambridge University Press. doi:10.1017/9781108779906.003

Steffen, R., & Steffen, H. (2021). Reactivation of Non-Optimally Orientated Faults Due to Glacially Induced Stresses. Tectonics, 40(11), e2021TC006853.

Stein, S., Cloetingh, S., Sleep, N. and Wortel R. (1989). Passive margin earthquakes, stresses and rheology. In S. Gregersen and P. Basham, eds., Earthquakes at North-Atlantic Passive Margins: Neotectonics and Postglacial Rebound, NATO ASI Series C 266, Springer, Dordrecht, pp. 231–259.

Stein, R. S. (1999), The role of stress transfer in earthquake occurrence, Nature, 402, 605-609.

Štěpančíková, P., et al. (2022), Acceleration of Late Pleistocene activity of a Central European fault driven by ice loading, Earth Planet. Sci. Lett., 591, 117596, https://doi.org/10.1016/j.epsl.2022.117596.

Taber, S. (1914). Seismic activity in the Atlantic coastal plain near Charleston, South Carolina. Bulletin of the Seismological Society of America, 4(3), 108-160.

Tamisiea, M., Mitrovica, J., & Davis, J. (2007). GRACE gravity data constrain ancient ice geometries and continental dynamics over Laurentia.Science, 316(5826), 881–883.

Tanaka S., 2010. Tidal triggering of earthquakes precursory to the recent Sumatra megathrust earthquakes of 26 December 2004 (Mw 9.0), 28 March 2005 (Mw 8.6), and 12 September 2007 (Mw 8.5), Geophys. Res. Lett., 37(2), doi:10.1029/2009GL041581.

Tapley, B. D., Bettadpur, S., Ries, J. C., Thompson, P. F., & Watkins, M. M. (2004). GRACE measurements of mass variability in the Earth system. science, 305(5683), 503-505.

Tay, C., Lindsey, E. O., Chin, S. T., McCaughey, J. W., Bekaert, D., Nguyen, M., ... & Hill, E. M. (2022). Sea-level rise from land subsidence in major coastal cities. Nature Sustainability, 1-9.

Trubienko, O., Garaud, J. D., & Fleitout, L. (2014). Models of postseismic deformation after megaearthquakes: The role of various rheological and geometrical parameters of the subduction zone. Solid Earth Discussions, 6(1), 427-466.

Tsai, V. C. (2011), A model for seasonal changes in GPS positions and seismic wave speeds due to thermoelastic and hydrologic variations, J. Geophys. Res., 116, B04404, doi:10.1029/2010JB008156.

Ueda, T., & Kato, A. (2019). Seasonal variations in crustal seismicity in San-in district, southwest Japan. GeophysicalResearch Letters, 46, 3172–3179. https://doi.org/10.1029/2018GL081789

Vachon, R., Schmidt, P., Lund, B., Plaza-Faverola, A., Patton, H., & Hubbard, A. (2022). Glacially Induced Stress Across the Arctic From the Eemian Interglacial to the Present—Implications for Faulting and Methane Seepage. Journal of Geophysical Research: Solid Earth, 127(7), e2022JB024272.

van Dam, T. M., G. Blewitt, and M. Heflin (1994), Detection of atmospheric pressure loading using the Global Positioning System, J. Geophys. Res., 99, 23,939– 23,950.

van Dam, T. M., and J. Wahr (1987), Displacements of the Earth's surface due to atmospheric loading: Effects on gravity and baseline measurements, J. Geophys. Res., 92, 1281– 1286.

vanDam, T. M., J. M. Wahr, P. C. D. Milly, A. B. Shmakin, G. Blewitt, D. Lavallee, and K. M. Larson (2001), Crustal displacements due to continental water loading, Geophys. Res, Lett., 28, 651–654.

van Dam, T., J. Wahr, and D. Lavallée (2007), A comparison of annual ver- tical crustal displacements from GPS and Gravity Recovery and Climate Experiment (GRACE) over Europe, J. Geophys. Res., 112, B03404, doi:10.1029/2006JB004335.

Vidale J.E., Agnew D.C., Johnston M.J., Oppenheimer D.H., 1998. Absence of earthquake correlation with earth tides: an indication of high preseismic fault stress rate, J. geophys. Res., 103(B10), 24 567–24 572..10.1029/98JB0059

Wahr, J. (1995), Earth Tides, Global Earth Physics, A Handbook of Physical Constants, AGU Washington, DC., Reference Shelf, 40– 46.

Wahr, J., S. A. Khan, T. van Dam, L. Liu, J. H. van Angelen, M. R. van den Broeke, and C. M. Meertens (2013), The use of GPS horizontals for loading studies, with applications to Northern California and southeast Greenland, J. Geophys. Res. Solid Earth, 118, 1795–1806, doi:10.1002/jgrb.50104.

Wang, R., & Kümpel, H. J. (2003). Poroelasticity: Efficient modeling of strongly coupled, slow deformation processes in a multilayered half-space. Geophysics, 68(2), 705–717. https://doi.org/10.1190/1.1567241

Wang, H., L. Xiang, L. Jia, L. Jiang, Z. Wang, B. Hu, and P. Gao (2012), Load Love numbers and Green's functions for elastic Earth models PREM, iasp91, ak135, and modified models with refined crustal structure from Crust 2.0, Comp. Geosci., 49, 190–199.

Wang, S., Xu, W., Xu, C., Yin, Z., Bürgmann, R., Liu, L., & Jiang, G. (2019). Changes in groundwater level possibly encourage shallow earthquakes in central Australia: The 2016 Petermann Ranges earthquake. Geophysical Research Letters, 46, 3189–3198. https://doi.org/10.1029/2018GL080510

Wetzler, N., Shalev, E., Göbel, T., Amelung, F., Kurzon, I., Lyakhovsky, V., & Brodsky, E. E. (2019). Earthquake swarms triggered by groundwater extraction near the Dead Sea fault. Geophysical Research Letters, 46(14), 8056-8063.

White, A. M., W. P. Gardner, A. A. Borsa, D. F. Argus, and H. R. Martens (2022), A Review of GNSS/GPS in Hydrogeodesy: Hydrologic Loading Applications and Their Implications for Water Resource Research, Water Resources Research, 58(7), e2022WR032078, doi:https://doi.org/10.1029/2022WR032078.

Whitehouse, P. L., M. J. Bentley, G. A. Milne, M. King, and I. D. Thomas (2012), A new glacial isostatic adjustment model for Antarctica: Calibrated and tested using observations of relatives sea level change and present day uplift rates, Geophys. J. Int., 190, 1464– 1482.

Wu, P. (1999), Modelling postglacial sea levels with power-law rheology and a realistic ice model in the absence of ambient tectonic stress, Geophys. J. Int., 139, 691– 702.

Wu, P., and Johnston, P., (2000), Can deglaciation trigger earthquakes in N. America?: Geophysical Research Letters, v. 27, p. 1323–1326, doi:10.1029/1999GL011070.

Wu, P., Steffen, R., Steffen, H., & Lund, B. (2021). Glacial Isostatic Adjustment Models for Earthquake Triggering. In H. Steffen, O. Olesen, & R. Sutinen (Eds.), Glacially-Triggered Faulting (pp. 383-401). Cambridge: Cambridge University Press. doi:10.1017/9781108779906.029.

Wu, P. C., Wei, M., & D'Hondt, S. (2022). Subsidence in coastal cities throughout the world observed by InSAR. Geophysical Research Letters, 49(7), e2022GL098477.

Wunsch, C., Heimbach, P., Ponte, R. M., Fukumori, I., & ECCO-GODAE CONSORTIUM MEMBERS. (2009). The global general circulation of the ocean estimated by the ECCO-Consortium. Oceanography, 22(2), 88-103.

Xu, X., Dong, D., Fang, M., Zhou, Y., Wei, N., & Zhou, F. (2017). Contributions of thermoelastic deformation to seasonal variations in GPS station position. GPS Solutions, 21(3), 1265–1274. https://doi.org/10.1007/s10291-017-0609-6

Xue, L., C. W. Johnson, Y. Fu and R. Bürgmann (2020), Seasonal Seismicity in the Western Branch of the East African Rift System. Geophys. Res. Lett., doi:10.1029/2019GL085882.

Yao, D., Y. Huang, L. Xue, Y. Fu, A. Gronewold, J. L. Fox (2022), Seismicity around Southern Lake Erie during 2013–2020 in Relation to Lake Water Level. Seismological Research Letters, doi: https://doi.org/10.1785/0220210343.

Young, Z. M., C. Kreemer, and G. Blewitt (2021), GPS Constraints on Drought-Induced Groundwater Loss Around Great Salt Lake, Utah, With Implications for Seismicity Modulation, J. Geophys. Res., 126(10), e2021JB022020, doi:https://doi.org/10.1029/2021JB022020.

Zaliapin, I., & Ben-Zion, Y. (2020). Earthquake declustering using the nearest-neighbor approach in space-time-magnitude domain. Journal of Geophysical Research: Solid Earth, 125(4),

e2018JB017120.

Zhai, Q., Peng, Z., Chuang, L. Y., Wu, Y. M., Hsu, Y. J., & Wdowinski, S. (2021). Investigating the impacts of a wet typhoon on microseismicity: A case study of the 2009 typhoon Morakot in Taiwan based on a template matching catalog. Journal of Geophysical Research: Solid Earth, 126(12), e2021JB023026.

Zhan, W., Heki, K., Arief, S., & Yoshida, M. (2021). Topographic amplification of crustal subsidence by the rainwater load of the 2019 typhoon Hagibis in Japan. Journal of Geophysical Research: Solid Earth, 126(6), e2021JB021845.

Zhuang, J., Y. Ogata, and D. Vere-Jones (2002), Stochastic declustering of space-time earthquake occurrences, J. Am. Stat. Assoc., 97, 369-382.